An anti-inflammatory transcriptional cascade conserved from flies to humans

Alexia Pavlidaki, Radmila Panic, Sara Monticelli, Céline Riet, Yoshihiro Yuasa, Pierre B Cattenoz, Brahim Nait-Oumesmar, Angela Giangrande, Angela Giangrande

Cell Reports

Article

An anti-inflammatory transcriptional cascade conserved from flies to humans

Graphical abstract

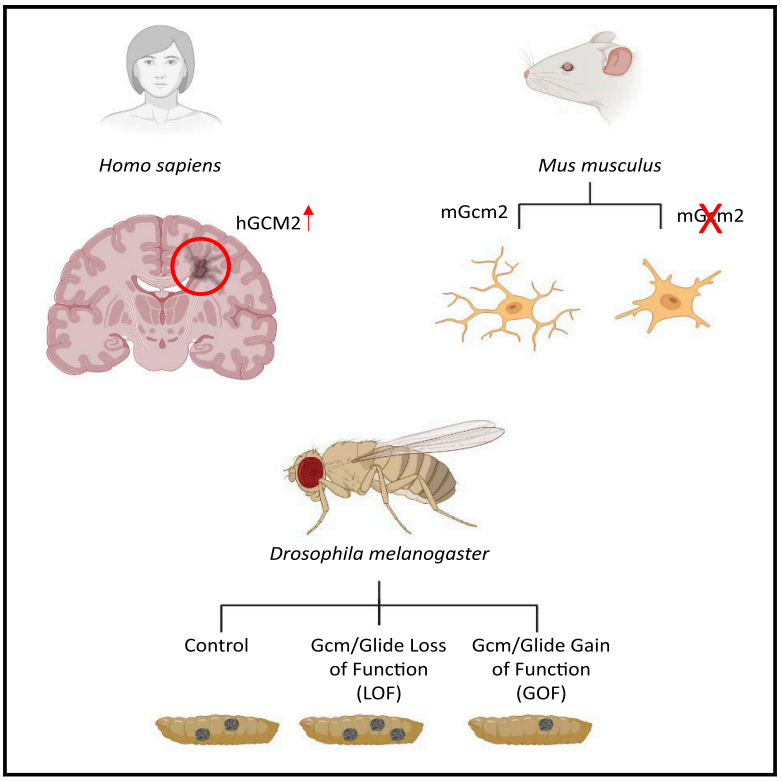

Highlights

- mGcm2 is expressed in murine microglia during chronic and acute inflammatory responses
- mGcm2 conditional knockout mice show an increased pro-inflammatory profile
- hGCM2 is expressed in microglia of patients with multiple sclerosis
- Gcm expression in hemocytes negatively controls the inflammatory state

Authors

Alexia Pavlidaki, Radmila Panic, Sara Monticelli, ..., Pierre B. Cattenoz, Brahim Nait-Oumesmar, Angela Giangrande

Correspondence

brahim.nait_oumesmar@upmc.fr (B.N.-O.), angela@igbmc.fr (A.G.)

In brief

Pavlidaki et al. show that the Gcm cascade has an evolutionary conserved role from flies to mice and humans. Deletion of Gcm leads to increased pro-inflammatory responses during acute and chronic inflammation in both mice and flies. Finally, GCM2 is present in acute inflammatory conditions in brain lesions in humans.

Pavlidaki et al., 2022, Cell Reports *41*, 111506
October 18, 2022
https://doi.org/10.1016/j.celrep.2022.111506

CellPress

Cell Reports

CellPress
OPEN ACCESS

Article

An anti-inflammatory transcriptional cascade conserved from flies to humans

Alexia Pavlidaki,[1,2,3,4,6] Radmila Panic,[5,6] Sara Monticelli,[1,2,3,4] Céline Riet,[1,2,3,4] Yoshihiro Yuasa,[1,2,3,4] Pierre B. Cattenoz,[1,2,3,4] Brahim Nait-Oumesmar,[5,7,*] and Angela Giangrande[1,2,3,4,7,8,*]

[1]Institut de Génétique et de Biologie Moléculaire et Cellulaire, Illkirch, France
[2]Centre National de la Recherche Scientifique, UMR7104, Illkirch, France
[3]Institut National de la Santé et de la Recherche Médicale, U1258, Illkirch, France
[4]Université de Strasbourg, Illkirch, France
[5]Sorbonne Université, Institut du Cerveau - Paris Brain Institute - ICM, Inserm, CNRS, APHP, Hôpital de la Pitié-Salpêtrière, Paris, France
[6]These authors contributed equally
[7]Senior author
[8]Lead contact
*Correspondence: brahim.nait_oumesmar@upmc.fr (B.N.-O.), angela@igbmc.fr (A.G.)
https://doi.org/10.1016/j.celrep.2022.111506

SUMMARY

Innate immunity is an ancestral process that can induce pro- and anti-inflammatory states. A major challenge is to characterize transcriptional cascades that modulate the response to inflammation. Since the *Drosophila* glial cells missing (Gcm) transcription factor has an anti-inflammatory role, we explored its regulation and evolutionary conservation. Here, we show that the murine Gcm2 (mGcm2) gene is expressed in a subpopulation of aged microglia (chronic inflammation) and upon lysophosphatidylcholine (LPC)-induced central nervous system (CNS) demyelination (acute inflammation). Moreover, mGcm2 conditional knockout mice show an increased inflammatory phenotype upon aging or LPC injection, and hGCM2 is expressed in active demyelinating lesions of patients with multiple sclerosis. Finally, *Drosophila* Gcm expression is induced upon aging and acute challenge, and its overexpression decreases the inflammatory phenotype. Altogether, these data indicate that the inducible Gcm cascade is conserved from flies to humans and represents a potential therapeutic target in the control of the inflammatory response.

INTRODUCTION

The immune response is one of the oldest processes of living organisms. It goes from simple enzymatic reactions in bacteria to cellular and humoral pathways in more complex animals (Buchmann, 2014; Dunin-Horkawicz et al., 2014). The main requirement for a successful immune response is the recognition of non-self through specific receptors that activate different immune pathways. It is controlled by either pro- or anti-inflammatory cues. The pro-inflammatory JAK/STAT, Toll, and nuclear factor κB (NF-κB) pathways are found in both insects and mammals (Fabian et al., 2021). The transforming growth factor β (TGF-β) signaling pathway is associated with promotion of anti-inflammatory properties in vertebrates upon resolution of inflammation, with similar molecules being present in flies (Clark et al., 2011; Fadok et al., 1998). One of the most challenging issues is to discover transcription factors that coordinately block the inflammatory response.

Glial cells missing/Glial cell deficiency (Gcm/Glide, Gcm throughout the text) is expressed early and transiently in the hemocytes of *Drosophila melanogaster*, functional orthologs of vertebrate macrophages (Bernardoni et al., 1997). *gcm* silencing in fly macrophages does not, on its own, produce an overt phenotype but enhances the inflammatory phenotype triggered by the constitutive activation of the JAK/STAT pathway (Bazzi et al., 2018; Cattenoz et al., 2016; Jacques et al., 2009) or even by an acute inflammatory challenge that is performed well after *gcm* expression has ceased. Thus, Gcm modulates acute and chronic inflammatory responses through mechanisms that are not fully understood.

Gcm is an atypical zinc finger transcription factor that is structurally conserved throughout evolution. The two mammalian orthologs are named *hGCM1* and *hGCM2* in humans and *mGcm1* and *mGcm2* in mice. *Gcm1* is required for the differentiation of trophoblasts in the developing placenta, and its mutation is associated with pre-eclampsia (Chiang et al., 2009). *Gcm2* is expressed and required mainly in the parathyroid glands, where it is necessary for the survival and differentiation of the precursor cells. No role was described in the immune cells (Gordon et al., 2001; Gunther et al., 2000; Kim et al., 1998). Since the fly *gcm* gene, but not its orthologs, is also necessary in glia (Cattenoz and Giangrande, 2015; Vincent et al., 1996), and since the fly glial cells constitute the immune cells of the nervous system, we speculated that this transcriptional pathway may have an anti-inflammatory role in microglia, the resident macrophages of the vertebrate nervous system. Microglia are not only responsible for the development and the homeostasis of the central nervous system (CNS) but are also involved in neuroinflammation

(Ransohoff, 2016). Moreover, recent studies suggest that the increased inflammation in the aged brain is attributed, in part, to the resident population of microglia (Spittau, 2017). The heightened inflammatory profile includes differences in morphology and gene expression of aged versus young microglia (Michell-Robinson et al., 2015; Perry et al., 1993) that are associated with a "sensitized" or "primed" phenotype. This might be triggered by transcriptional pathways controlling the inflammatory response.

Here, we show that the murine ortholog *mGcm2* starts being expressed in a subset of microglia upon aging. Loss of *mGcm2* enhances the aging phenotype in terms of active microglia morphology and expression of pro-inflammatory markers, corroborating the hypothesis that this transcription factor has an anti-inflammatory role during chronic inflammation. Furthermore, *mGcm2* expression is induced in demyelinated lesions triggered by lysophosphatidylcholine (LPC) injection in the spinal cord, and in *mGcm2*-inducible conditional knockout animals, the same challenge triggers a much stronger inflammatory reaction. Therefore, *mGcm2* is involved in chronic and acute responses. Importantly, the human ortholog *hGCM2* is expressed in active demyelinating lesions of patients with multiple sclerosis (MS). Finally, chronic and acute challenges induce the expression of *gcm* in flies. *De novo* expression of *gcm* counteracts the inflammatory phenotype, hence explaining its mode of action. Altogether, our data demonstrate that Gcm constitutes a highly conserved immune transcriptional cascade from flies up to humans and represents a potential therapeutic target in the control of the inflammatory response.

RESULTS

Expression of the murine *Gcm* genes *in vitro*

We assessed whether the *mGcm1* and *mGcm2* genes are expressed in microglia by characterizing CNS primary cultures (Nait-Oumesmar et al., 2000; Peissig et al., 2018). Microglia were labeled with the broad hematopoietic marker CD45 (Denes et al., 2015). Microglia adopt one of the three morphologies both *in vitro* and *in vivo*: ramified microglia with small cell body and long ramifications, round cells with a small cell body and no ramifications, or amoeboid microglia with a big cell body and no ramifications (Bohatschek et al., 2001; Leyh et al., 2021; Thored et al., 2009). Round cells are considered active microglia and the other two as resting cells (Ovanesov et al., 2006). mGcm2, but not mGcm1, is specifically expressed in 30% of round-shaped microglia (Figures S1A and S1B). We ascertained the specificity of the mGcm2 immunolabeling in a conditional knockout (cKO) $mGcm2^{flox/flox}$ mouse line crossed with the *Cx3cr1-Cre* line expressing Cre recombinase in microglia. The $mGcm2^{flox/flox}$ line was produced by introducing two LoxP sites upstream and downstream of the *Gcm* exons 2, 3, and 4. mGcm2 labeling is absent in the cKO microglia, proving, by the same token, the specificity of the antibody and the efficiency of our cKO model.

In sum, mGcm2 is expressed in active microglia of CNS cultures.

mGcm2 is expressed in the microglia of aged animals

Based on the above results, we analyzed neonatal microglia at postnatal day 14 (P14) but found no mGcm2 expression (Figure 1A). This could be explained by the fact that, *in vivo*, microglia display major differences from microglial cultures (Butovsky et al., 2014). The finding that mGcm2 expression is specific to active microglia *in vitro* prompted us to ask whether its expression is induced in an inflammatory condition such as aging. Brain and spinal cord were collected at different ages: P14 and 2, 12, and 24 months. As cell-specific markers, we used the microglia-specific cocktail (CD11b, CD68, F4/80) that distinguishes microglia from the meningeal macrophages (Rangaraju et al., 2018). mGcm2 is expressed in microglia at 12 and 24 months, but not in 2-month-old animals, in different areas of the brain including the cortex (Figure 1A). The number of $mGcm2^{+}$ microglia increases over time: 12- and 24-month-old cortices show 25% and almost double $mGcm2^{+}$ microglia (48%), respectively (Figure 1B).

We also performed RNA *in situ* hybridization (ISH) on brain sections and confirmed that *mGcm2* is expressed in aged brains (18-month-old animals), while *mGcm1* is not expressed in either control or cKO brains (Figures S1C and S1D). This further validates the efficiency of our flox/flox mutant line and shows that *mGcm1* does not compensate for the lack of *mGcm2* expression. Finally, to evaluate the expression in other resident macrophages, lung and adipose tissues were dissected from 24-month-old animals, and cryo-sections were labeled for CD45 and mGcm2. No mGcm2 labeling was observed in the resident macrophages associated with those tissues (Figure S1E).

Thus, mGcm2 is expressed only in a subset of aged microglial cells.

Microglia of *mGcm2* cKO mice have an active morphology in homeostatic conditions

To explore the role of mGcm2 in microglia *in vivo*, we characterized their morphology, which is tightly linked to the activation state: resting cells have long ramifications, while active cells have shorter ramifications (Heindl et al., 2018). Sections of control and cKO brains from different age groups were labeled with the microglial marker Iba1 (Cengiz et al., 2019) (Figure 1C). Our criteria include the number of ramifications and the coverage area of the cell, that is, the area to which microglia extend their ramifications, which thus represents the area they can survey. The former parameter is a direct measurement of their activation state, while the latter is an indirect indicator, as active microglia have shorter or less ramifications, which results in a decreased coverage area.

We found that microglia morphology changes over time but more so in cKO animals (Figures 1D and 1E). More specifically, the number of ramifications per cell decreases during aging in both genotypes. However, there is a significant decrease in the number of ramifications in *mGcm2* cKO compared with control microglia at 24 months (Figure 1D). The same trend is also visible for the coverage area (Figure 1E).

These data reveal that the lack of *mGcm2* has an impact on microglia morphology, indicative of a pro-inflammatory phenotype.

mGcm2 cKO animals display a pro-inflammatory profile

We complemented the morphological data by labeling 2-, 12-, and 24-month-old brains with pro- and anti-inflammatory

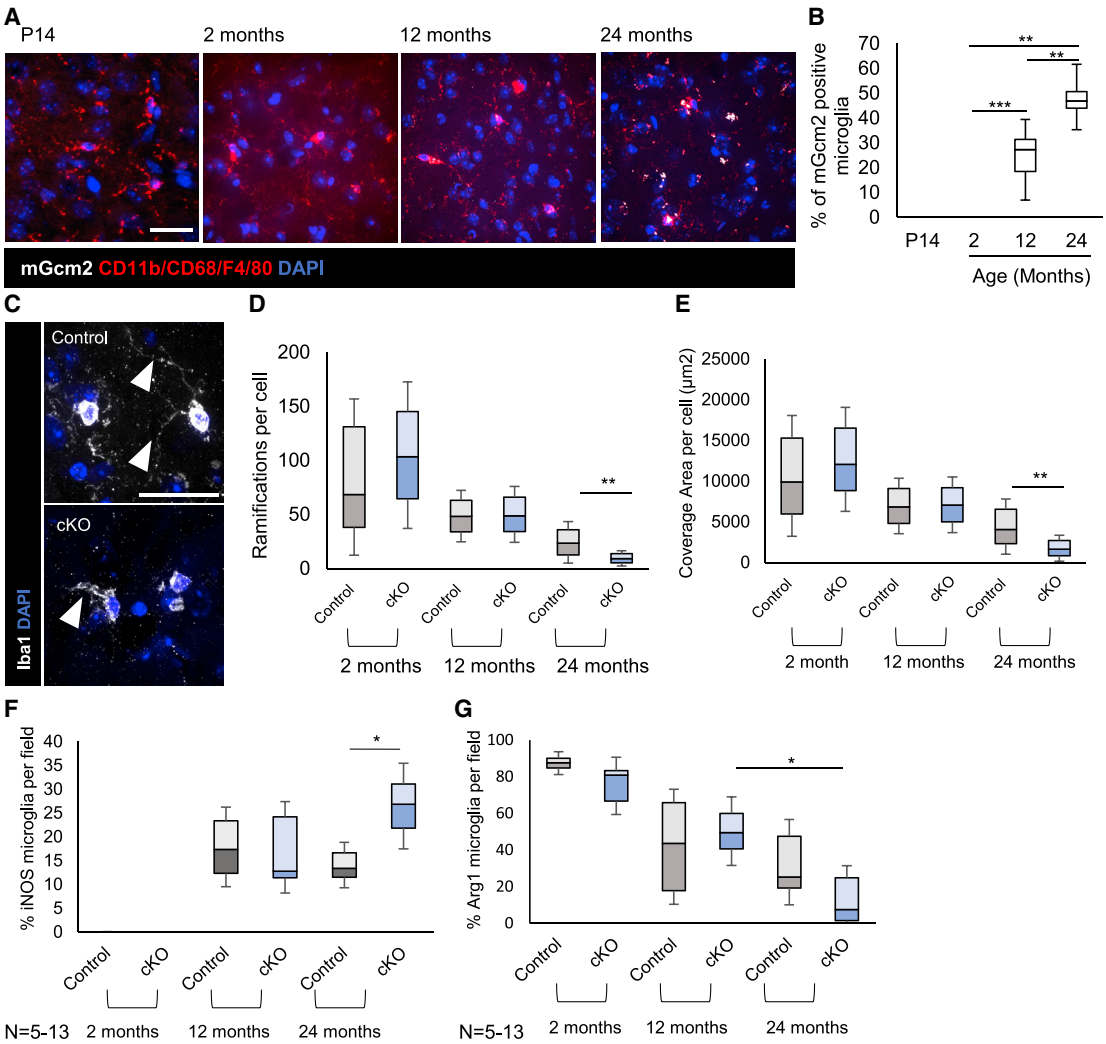

Figure 1. mGcm2 expression *in vivo* and impact of its deletion upon aging

(A) Immunolabeling of brain sections for mGcm2 expression at P14 and in 2-, 12-, and 24-month-old animals. mGcm2 (gray), microglia (CD68, CD11b, F4/80, red), and DAPI (blue). n = 5–13, genotype; scale bar: 50 µm.

(B) Quantification of mGcm2$^+$ microglia in the cortex at different ages.

(C) Microglia immunolabeling of brain sections with Iba1 (gray) and DAPI (blue) at 24 months. Scale bar: 50 µm.

(D and E) Analysis of microglia morphology in 2-, 12-, and 24-month-old animals of the different genotypes for number of ramifications (D) and coverage area (µm^2) (E).

(F and G) Quantification of the (F) pro-inflammatory microglia (iNOS$^+$) and (G) anti-inflammatory microglia (Arg1$^+$). n = 5–13; *p < 0.05, **p < 0.01, and ***p < 0.001. Statistical significance was determined by two-way ANOVA, followed by two-tailed, unpaired t test. *Cx3cr1-Cre*$^{+/-}$*;mGcm2*$^{flox/+}$ (control) and *Cx3cr1-Cre*$^{+/-}$*;mGcm2*$^{flox/flox}$ (cKO).

markers. Microglia/macrophage activation states are classified as pro-inflammatory (or M1) or anti-inflammatory (or M2). The M1 microglia is typified by the production of inflammatory cytokines and reactive oxygen species, while the M2 microglia take on an anti-inflammatory phenotype involved in wound repair and debris clearance (Colton, 2009; Gordon, 2003). Upon aging, where neuroinflammation is a prominent feature, M2 microglia decrease in number, and M1 microglia increase. We chose the markers inducible nitric oxide synthase (iNOS) for the M1 state and Arginase-1 (Arg1) for the M2 state, which were already used to characterize aging microglia *in vivo* (Lisi et al., 2017). Labeling from different age groups shows that iNOS is present mostly in 12- and 24-month-old animals, and its expression increases in both groups as they age (Figures 1F and S2A). Upon quantification, we found that *mGcm2* cKO animals specifically display an increased number of iNOS$^+$ microglia compared with control animals by 24 months.

Next, we evaluated the number of Arg1$^+$ cells (Figures 1G and S2B). Two-month-old control animals have a higher number of Arg1$^+$ microglia compared with 12- and 24-month-old animals. Likewise, *mGcm2* cKO animals show a significant decrease in the number of Arg1$^+$ microglia, from 2 (74%) to 12 months

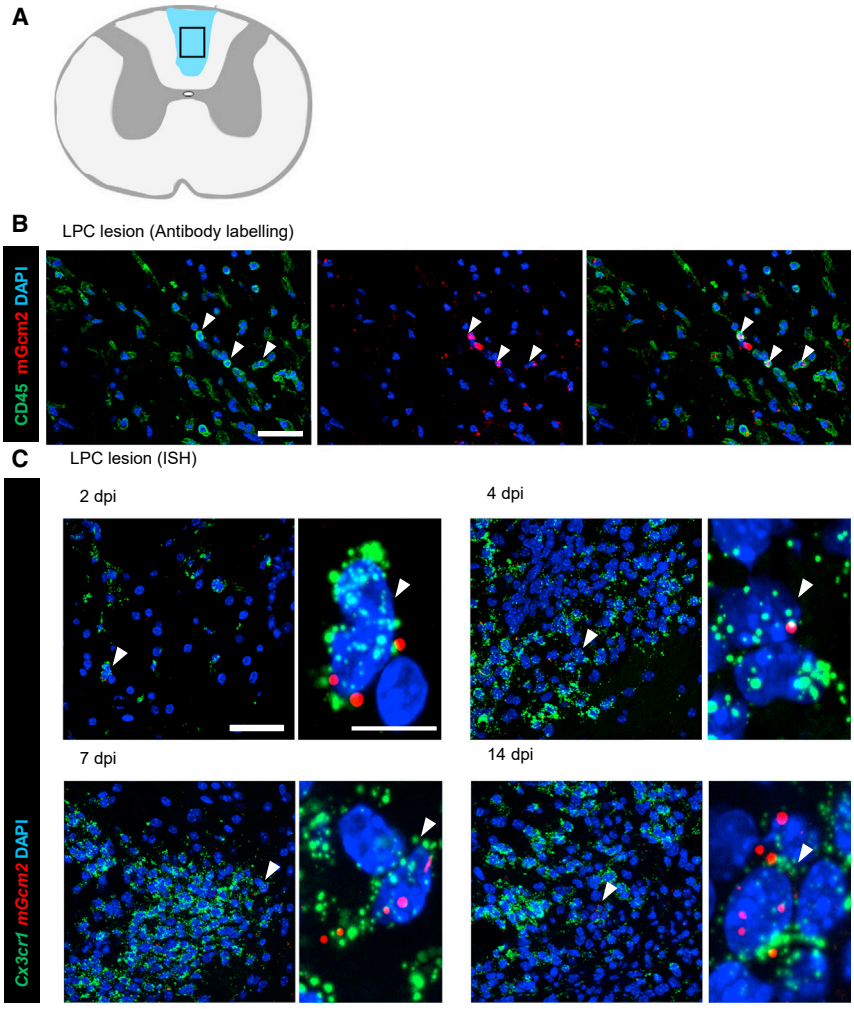

Figure 2. mGcm2 expression in LPC lesions of mouse spinal cord

(A) Schematic representation of the LPC demyelinated lesion (blue) in the dorsal white of the mouse spinal cord at 2 dpi. The dashed box indicates the location of mGcm2^{+}CD45^{+} cells shown in (B).

(B) Immunolabeling of brain sections for CD45 (green) and mGcm2 (red) in the spinal cord at 2 dpi. Double-positive cells with nuclear mGcm2 expression are indicated by arrows.

(C) RNA ISH of spinal cord sections. *mGcm2* (red) are mainly detected in a subset of microglia/macrophages expressing *Cx3cr1* (green) at 2, 4, 7, and 14 dpi. Nuclei are counterstained with DAPI (blue). n = 5 animals per time point.

Scale bars: (B) 20 μm; (C) 50 μm and 10 μm.

(47%). Importantly, only the percentage of Arg1^{+} microglia in the cKO animals further decreases from 12 to 24 months, resulting in a significant decline (Figure 1G). Thus, the microglia lacking *mGcm2* display a stronger progression toward a pro-inflammatory phenotype compared with control microglia.

The state of other CNS populations does not seem overtly affected in the mutant animals. The size of astrocytes increases in inflammatory conditions, a phenomenon called reactive astrogliosis that can be measured via GFAP labeling (Rodriguez et al., 2009). We found no difference between the GFAP labeling of 24-month-old control and mutant animals (Figures S3A and S3B). Similarly, we found no difference in neuronal cell death by co-labeling the cell death marker caspase 3 with the pan-neuronal marker NeuN (Figures S3C–S3E). No difference in oligodendrocyte number was found either (Figures S3F and S3G). Accordingly, mutant and control animals show similar behavioral habits in an open-field test (Figures S3H–S3J), which assays general locomotor activity levels, anxiety, and willingness to explore.

The morphological and molecular data show that *mGcm2* has an anti-inflammatory role in murine microglia during chronic inflammatory conditions such as aging.

mGcm2 is expressed in acute LPC lesions

Since *mGcm2* expression is induced upon aging, we asked whether it is also expressed in immune cells following CNS injury, which represents a condition of acute inflammation. We induced acute demyelination by LPC injection in the mouse dorsal white matter spinal cord and analyzed the *mGcm2* expression profile (Figure 2A). LPC lesions show a limited amount of inflammation, usually associated with myelin debris removal. The mGcm2 protein was specifically detected in a subset of CD45^{+} immune cells (Figure 2B). RNAscope ISH assays also show *mGcm2* labeling in very few microglia/macrophages, specifically within the lesions from 2 to 21 days post-infection (dpi) (Figure 2C). In sum, *mGcm2* gene expression is upregulated in demyelinating lesions in a subset of cells belonging to the microglia/macrophage lineages.

Loss of *mGcm2* in microglia promotes a pro-inflammatory response after demyelination

To decipher the functional role of *mGcm2* in microglia/macrophages in LPC lesions, we generated a temporally inducible cKO mouse line. The *mGcm2* floxed strain (Figure 3A) was crossed with the $CX_{3CR1}^{CreER/+}$ mouse line (Parkhurst et al., 2013). The deletion was induced in the F1 generation, specifically in microglia by tamoxifen injection (Figure 3B). We refer to this mouse strain as $CX_{3CR1}^{CreER/+}$;$Gcm2^{flox/flox}$ (inducible cKO [icKO]). $CX_{3CR1}^{CreER/+}$;$Gcm2^{flox/+}$ heterozygous littermates (named control thereafter) and $Gcm2^{flox/flox}$ and wild-type (WT) animals were used as controls for LPC lesions. Ten- to sixteen-week-old mice were treated with tamoxifen during 5 consecutive days prior to LPC-induced lesions. We then assessed the impact of *mGcm2* deletion in microglia/macrophages on the different steps of the remyelination process, including oligodendrocyte precursor cell (OPC) recruitment, differentiation, and remyelination (Figure 3B). *mGcm2* deletion was

CellPress
OPEN ACCESS

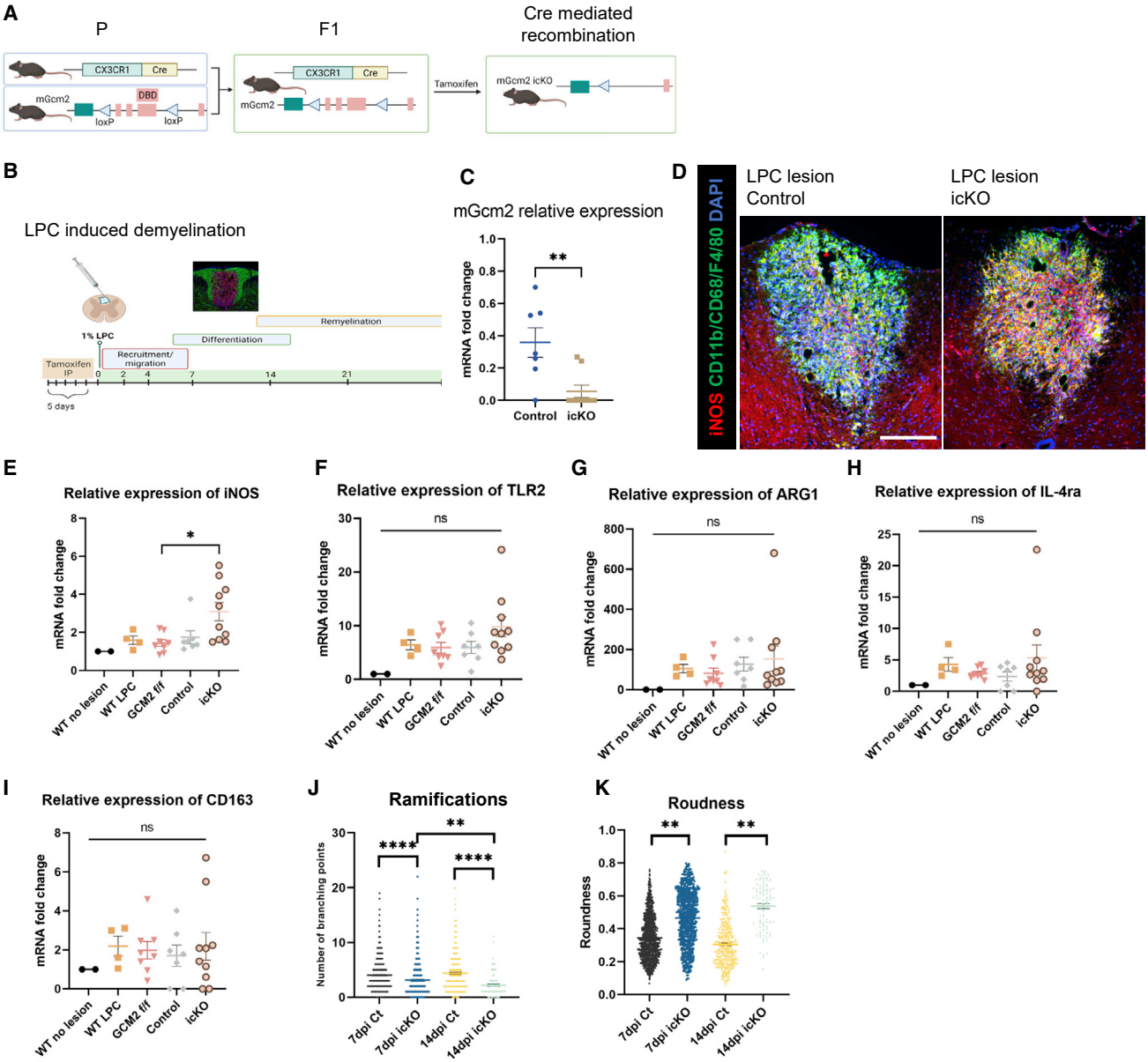

Figure 3. Loss of mGcm2 function in microglial cells favors a pro-inflammatory state after demyelination

(A) Schematic representation of the $CX_{3CR1}^{CreER/+}$ transgene and mGcm2 floxed allele, and strategy used to generate tamoxifen-inducible mGcm2 (icKO) in microglia. Created with BioRender.com.

(B) Schematic illustration of LPC-induced demyelination in the mouse spinal cord dorsal funiculus, and typical time frame of OPC migration/recruitment, differentiation and remyelination. Created with BioRender.com.

(C) mGcm2 gene expression in demyelinated spinal cords of $CX_{3CR1}^{CreER/+}$;$mGcm2^{flox/+}$ (icKO) and $CX_{3CR1}^{CreER/+}$;$mGcm2^{flox/flox}$ (control) mice at 4 dpi. mGcm2 mRNA fold changes were normalized relative to demyelinated WT spinal cords at the same time point. Data represent mean + SEM. Mann-Whitney U non-parametric test was used for the statistical analysis (n = 7–8/group). $^{**}p < 0.01$.

(D) Immunolabeling for M1 marker iNOS (red) and CD11b/ F4/80/ CD68 microglia/macrophages (green) in the LPC lesion of control and *mGcm2* icKO at 14 dpi. The number of microglia/macrophages expressing iNOS in LPC lesions increases in *mGcm2* icKO animals with respect to control.

(E–I) qPCR analysis of the relative gene expression of M1 and M2 macrophages markers in WT without LPC lesion and LPC demyelinated spinal cords of WT, $Gcm2^{flox/flox}$, control, and *mGcm2* icKO mice.

(J–K) Morphological analysis of $Iba1^{+}$ cells/macrophages with Visiopharm, in LPC lesions of control and *mGcm2* icKO animals, at 7 and 14 dpi. Two macrophages morphological parameters were evaluated: the number of ramifications (J) and the roundness (K).

Statistical analyses were performed with R and GraphPad software using one-way ANOVA in (E)–(I) and two-way ANOVA in (J) and (K), followed with Tukey's post hoc test. $^{*}p < 0.05$, $^{**}p < 0.01$, $^{****}p < 0.0001$. Scale bar: (D) 200 μm.

confirmed by qPCR analysis of RNA extracted from dissected spinal cord lesions at 4 dpi. *mGcm2* relative mRNA expression is indeed severely reduced in LPC demyelinated spinal cords of icKO mice with respect to controls (Figure 3C).

Next, we monitored the microglia response to LPC lesions in *mGcm2* icKO mice. Immunohistochemistry for iNOS combined with the microglia cocktail markers (CD11b, F4/80, and CD68) revealed a drastic increase of microglia/macrophages in a pro-inflammatory state in demyelinated lesions of *mGcm2* icKO mice compared with controls (Figure 3D). Initially, we performed qPCR analyses of M1 and M2 marker relative expression. In agreement with the immunohistochemistry data, as well as the aging data, the expression of the M1 genes *iNOS* (Figure 3E) and *TLR2* (Figure 3F) revealed a trend increase after spinal cord demyelination in the icKO mouse strain with respect to WT, $mGcm2^{flox/flox}$, and control mice. We also evaluated the relative gene expression of the M2 markers *Arg1* (Figure 3G), *Il-4ra* (Figure 3H), and *CD163* (Figure 3I) in *mGcm2* icKO and control animals; however, our data did not reveal any significant difference.

Next, we examined microglia/macrophages cell morphology in conditional *mGcm2* icKO and control mice in LPC demyelinated lesions *in vivo*. Spinal cord sections throughout the demyelinated lesions were labeled with Iba1, and the cell/macrophages morphology was evaluated with VisioPharm (Gober et al., 2022). The number of ramification points per Iba1+/macrophages cell decreases significantly in *mGcm2* icKO compared with controls, specifically in demyelinated lesions at 7 and 14 dpi (Figure 3J). As an additional morphological parameter of activated microglia/macrophages, we evaluated the roundness of the cells at the same time points. The number of macrophages exhibiting a round morphology increases significantly in *mGcm2* icKO compared with controls (Figure 3K), further indicating that *mGcm2* loss of function in microglia/macrophages favors a pro-inflammatory state.

The above findings support a role of *mGcm2* as an anti-inflammatory transcription factor in mouse microglia/macrophages under pathological conditions.

Loss of *mGcm2* in microglia delays oligodendrocyte differentiation in demyelinated lesions

The state of microglia activation plays a critical role in the regulation of demyelination and remyelination (Miron et al., 2013). Therefore, we asked whether *mGcm2* loss of function in microglia hampers myelin debris clearance and oligodendrocyte differentiation in LPC-induced demyelinated lesions. Oil red O staining was performed to evaluate the density of microglia/macrophages containing myelin debris (Figure S4A). The Oil red O^+ area, as well as the percentage of the oil red O^+ area, in LPC lesions did not differ significantly between *mGcm2* icKO and control mice at similar time points post-demyelination (Figures S4B and S3C), suggesting that *mGcm2* deletion in microglia/macrophages does not affect the ability of these cells to phagocyte myelin debris.

We next examined whether oligodendrocyte differentiation could be hampered. Spinal cord sections of demyelinated lesions from icKO and control mice were immunolabeled for Olig2, a pan-oligodendrocyte marker, together with CC1, a specific marker of differentiated oligodendrocytes (Figure S4D). Quantification of the percentage of $Olig2^+CC1^+$ mature oligodendrocytes and $Olig2^+CC1^-$ OPCs revealed a significant increase of differentiated oligodendrocytes in both groups at 7 and 21 dpi (Figures S4E–S4G). Nevertheless, oligodendrocyte differentiation is delayed in LPC lesions of the *mGcm2* icKO strain, with respect to controls, between 7 and 14 dpi (Figures S4E and S4F). It is worth noting that the overall number of $Olig2^+$ oligodendroglial cells in demyelinated lesions increases in both groups but was significantly lower in the icKO mice compared with the controls at 21 dpi (Figures S4E and S4G), suggesting that the pro-inflammatory state of *mGcm2* icKO microglia/macrophages hampers oligodendroglia cell survival or apoptosis.

hGCM2 is expressed in active MS lesions

To assess the relevance of these findings in humans, we analyzed the expression of *hGCM2* in acute and chronic MS lesions, as well as in the normal-appearing white matter from MS and non-neurological control cases (Table S1). MS lesion subtypes were characterized using Luxol Fast Blue and major histocompatibility complex (MHC) class II staining (Figure 4A) and were classified as active, chronic active, and chronic inactive (Nait-Oumesmar et al., 2007). The hGCM2 protein was specifically detected in few MHC class II^+ immune cells located in active MS lesions, which have traditionally been defined as showing demyelination with inflammatory infiltrates, whereas chronic lesions show demyelination with little or no activity (Figure 4B). We next performed double RNA ISH for *hGCM2* and *hCD68* and found *hGCM2* expression in few $hCD68^+$ cells/macrophages only in active lesions and in the active rim of chronic active lesions (Figure 4C).

gcm expression is induced upon aging in *D. melanogaster*

Since the Gcm pathway is induced in chronic (aging) and acute (LPC-induced) inflammatory conditions in mice, we asked whether this is an ancestral process and evaluated it in aged *Drosophila* brains. Normally, Gcm is expressed in a subpopulation of hemocytes, in which it has an anti-inflammatory role. Gcm expression is confined to the hemocytes derived from the primitive hematopoietic wave that occurs in the procephalic mesoderm of the embryo (Cattenoz and Giangrande, 2015). These hemocytes cease to express Gcm by the end of embryogenesis and survive to adulthood, where they co-exist with those derived from the second wave occurring in the larval lymph gland, which is Gcm independent (Lan et al., 2020).

In the adult, hemocytes are mostly associated with peripheral tissues (Cattenoz et al., 2021); we therefore assessed the number of brain-associated hemocytes over time by labeling dissected fly brains with macrophage markers (P1/NimC4 and Hemese) at different ages, from week 1 (young animals) to 6 (old animals) (Figures 5A and 5B). The number of brains that display associated hemocytes increases over time, and by 6 weeks, all brains are associated with hemocytes (Figure 5C). Furthermore, the number of hemocytes increases from week 1 to 5 (Figure 5D). The number of brain-associated hemocytes observed in each animal varies, which likely depends on the dissection protocol: cells that can

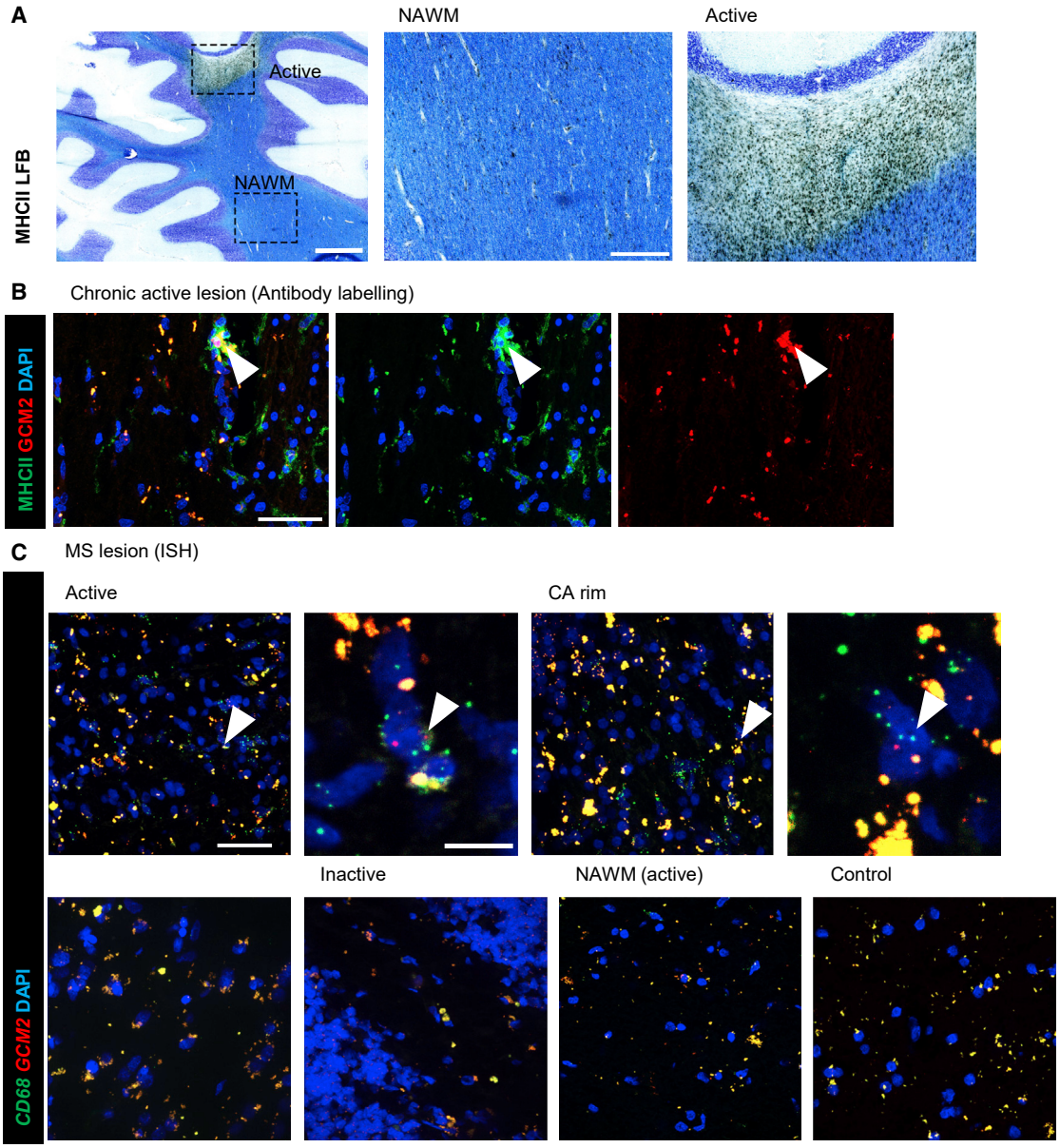

Figure 4. hGCM2 is expressed in microglia in active lesions of patients with MS

(A) Luxol fast blue (LFB)/MHC class II staining showing a typical active MS lesion in the cerebellar white matter. The boxed areas illustrate an active lesion containing MHCII^{+} immune cells and the normal-appearing white matter (NAWM).

(B) Immunolabeling for MHC class II and hGCM2 in an active lesion. Note that hGCM2 expression is only detected in few MHC class II^{+} immune cells (arrow) of active MS lesions.

(C) RNA ISH for *hGCM2* and *hCD68* microglial marker in active plaques, the active rim, chronic core of chronic active lesions, chronic inactive lesions, NAWM of MS, and control cases. *hGCM2* transcripts are only detected in few *hCD68*-expressing microglial cells located in active lesions and not in inactive lesions nor in NAWM of MS or control cases.

Note that the yellow dots in (B) and (C) are due to lipofuscin aggregates that are inherent to human brain tissue. n = 1–2 samples per condition. Scale bars: (A) 2 mm and 500 μm for magnification; (B and C) 50 μm 10 μm.

migrate as hemocytes may dissociate from the brain. We next assessed the expression profile of *gcm* in the adult brain upon aging by performing ISH. In young animals, *gcm* is expressed only in two neuronal clusters, located in the central brain at lateral and dorsal positions (Soustelle and Giangrande, 2007). In 6-week-old animals, however, *gcm* labeling is present at ectopic positions, indicating *de novo* expression (Figure 5E). As in the case of the hemocyte markers, *gcm* labeling is located at the surface of and not within the brain, indicative of cells that are associated with, but do not belong to, the tissue itself.

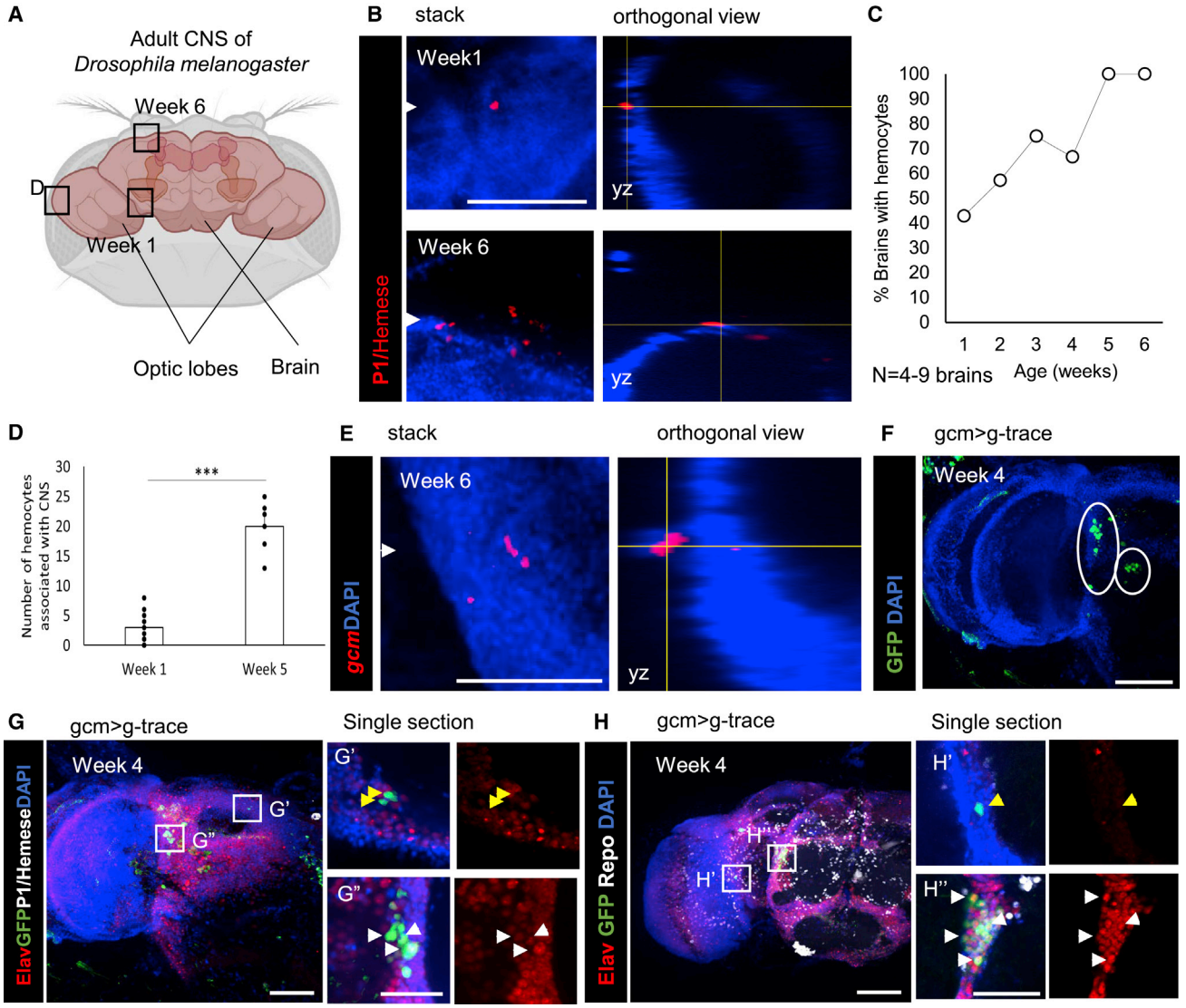

Figure 5. Hemocytes and *gcm* expressing cells associated with the aging *Drosophila* CNS

(A) Schematic of the adult *Drosophila* brain, which contains the medially located central complex and the lateral optic lobes. The squares indicate the positions of (B) and (D).

(B) Hemocytes associated with the brain at different ages, from weeks 1 and 6 at 25°C. The rectangular panels show orthogonal projections along the yz axes from the position indicated by the white arrowheads.

(C) Percentage of brains with associated hemocytes at different ages. n = 4–9 brains.

(D) Quantification of hemocytes that are associated with the brain at weeks 1 and 6.

(E) RNA ISH showing ectopic *gcm* expression in the aged brain; the orthogonal view shows that the signal is in cells closely associated with the brain but not within it. Scale bar: 50 μm.

(F) Immunolabeling of adult *Drosophila* brain with *gcm* tracing (*gcm > g-trace*) in green and DAPI (blue). Scale bar: 50 μm. The circles indicate the two neuronal clusters that express *gcm*.

(G) Immunolabeling of adult *Drosophila* brain with *gcm* tracing (*gcm > g-trace*) in green, P1/Hemese (gray), Elav (red), and DAPI (blue), Scale bar: 20 μm.

(H) Immunolabeling of adult *Drosophila* brain with *gcm* tracing (*gcm>g-trace*) in green, Repo (gray), Elav (red), and DAPI (blue). Scale bar: 20 μm. The white arrowheads indicate GFP$^+$ cells that express Elav, and the yellow arrowheads indicate GFP$^+$ cells that do not express Elav.

(F–H) The brains are from animals of week 4 at 29°C. n = 5–10 brains per labeling (see STAR Methods).

The *in situ* assay identifies cells that express *gcm* at the time of the dissection. Since *gcm* expression in the old hemocytes might be a transient process, this approach may miss cells that have expressed *gcm* earlier. For this reason, we performed lineage tracing using the g-trace tool and followed all the cells that express and/or have expressed *gcm* at some point (Evans et al., 2009). This may reveal more *gcm*$^+$ cells than the *in situ* assay. To make sure that we specifically look at *de novo* expression

and not at remnant expression from the embryonic hemocytes, we activated the g-trace only after adult eclosion (Figures 5F and S5A–S5C). The results show *gcm*$^+$ cells that are associated with the brain and do not express glial or neuronal markers. Surprisingly, these cells do not express the P1/Hemese pan-hemocyte markers either (Figures 5G and 5H). Most of the GFP$^+$ cells are located outside the CNS, and some are within. Recent studies have shown that under neuroinflammation, adult hemocytes are capable of crossing the blood-brain barrier (Winkler et al., 2021). Furthermore, a single cell study of old fly CNS showed a cluster that has hemocyte markers, thus suggesting the close proximity of hemocytes with the aging CNS (Davie et al., 2018). Of note, both the immunofluorescence and the *in situ* assays reveal only a few cells that are *gcm*$^+$ or GFP$^+$, which confirms that there is only a subpopulation that expresses this transcription factor and that this expression is stable.

gcm expression is induced upon acute challenge and counteracts the inflammatory state

Based on the above results, we asked whether *gcm* is also reactivated upon an acute inflammatory challenge. In *Drosophila*, the most studied acute inflammatory response is induced by wasp patriotization. In brief, the parasitoid wasp *Leptopilina boulardi* is allowed to infest and lay eggs in *Drosophila* larvae. This leads to extensive hemocyte proliferation and activation, which consists of resting hemocytes transdifferentiating into lamellocytes (activated hemocytes) in the infested larvae (Kim-Jo et al., 2019). Lamellocytes are huge cells able to encapsulate the wasp egg, preventing it from hatching and hence allowing *Drosophila* to escape the infestation. Upon activating the g-trace tool only during the larval life, no *gcm* expression can be detected in normal conditions in third-instar larvae (Figure S5D). Upon wasp infestation, however, *gcm* (g-trace)$^+$ cells surround the wasp eggs, revealing a *de novo* expression of *gcm* following the acute challenge (Figure 6A). We also found *gcm* expression in circulating blood cells, and these cells correspond to lamellocytes, which express phalloidin at high levels (Figure 6B). Thus, *gcm* expression is induced by an acute inflammatory challenge.

Since *gcm* is expressed *de novo* upon wasp infestation, we asked whether *gcm* gain or loss of function (GOF or LOF, respectively) affects the inflammatory response. The extensive hemocyte proliferation induced by wasp infestation triggers the formation of the so-called melanotic tumors, masses of aggregated hemocytes that are melanized. We specifically induced (GOF) or silenced (LOF) *gcm* expression in the larval hemocytes after wasp infestation (Figure 6C) and evaluated the tumor phenotype as a readout of the inflammatory response. The infested animals of the three genotypes (control, LOF, and GOF) carry tumors, but their number and/or size varies. Large tumors contain the wasp eggs encapsulated by the fly hemocytes, while small/medium size tumors are due to hemocyte aggregation. LOF animals have, on average, more tumors than control and GOF animals (Figure 6D). This is mostly due to a very large increase in the number of small tumors (Figures 6E and 6F). GOF animals, on the other hand, show fewer large tumors compared with control animals.

In sum, silencing the *de novo* expression of *gcm* aggravates the inflammatory phenotype, and inducing *gcm* expression *de novo* ameliorates it.

gcm downregulation triggers a pro-inflammatory state in the *Drosophila* hemocytes

Altogether, our data indicate that the conserved Gcm pathway is induced in response to a wide variety of challenges and counteracts acute, as well as chronic, inflammation. It seemingly has a priming role: the cKO mice are fully viable and fertile and do not display an overt inflammatory phenotype, like the mutant flies (Bazzi et al., 2018). To investigate the molecular mechanisms underlying this priming process, we proceeded to do a high-throughput analysis in flies, given the simplicity of this animal model. Since Gcm is also involved in gliogenesis and its mutation is embryonic lethal, we analyzed the transcriptome of *srp(hemo)Gal4*;*UASgcmRNAi* (*gcmKD*) animals in which Gcm is specifically affected in hemocytes. *gcmKD* hemocytes present overall increased levels of expression of immune-related genes, such as anti-microbial peptides and components of major immune pathways (Figure 7A). In the embryo, the different expression is restricted mostly to STAT92E and Toll, but in the larva, more genes appear to have different expression levels between *gcmKD* and control hemocytes. The highest difference is found in Gene Ontology (GO) terms associated with immune regulation, such as regulation of immune response to bacteria and signaling pathway of recognition of peptidoglycans (Figure 7B).

Thus, silencing *gcm* triggers a transcriptional landscape indicative of a pro-inflammatory state.

DISCUSSION

The present study identifies an evolutionarily conserved anti-inflammatory transcriptional pathway. The Gcm transcription factor was known to regulate the development of fly immune cell populations (glia and hemocytes) and to modulate the inflammatory response. Here, we demonstrate that the expression of fly and murine *Gcm* genes is induced upon challenge, which helps counteract chronic and acute inflammatory states. Moreover, the human *Gcm2* ortholog is expressed in active MS lesions. The identification of this conserved pathway opens exciting perspectives to study neuroinflammatory diseases.

Aging results in gradual loss of normal function due to changes at the cellular and molecular level (Lopez-Otin et al., 2013). Microglia exhibit an exaggerated pro-inflammatory response during aging, a phenomenon referred to as microglia priming (Michell-Robinson et al., 2015; Perry et al., 1993). Morphologically, aged microglia have enlarged processes, cytoplasmic hypertrophy, and a less ramified appearance (Damani et al., 2011; Tremblay et al., 2012). They also express higher levels of activation markers than young microglia (Conde and Streit, 2006). All these changes are associated with decreased number of microglia in an anti-inflammatory state (Miron et al., 2013). Our data indicate that *mGcm2* expression helps keep the inflammatory state under control during aging. Furthermore, they show a statistically significant increase of the pro-inflammatory marker *iNOS* and a significant decrease of the anti-inflammatory marker *Arg1* between 12 and 24 months. *mGcm2* hence regulates the activation state in microglia, and the loss of its expression leads to an uncontrolled stimulation with a higher pro-inflammatory profile even under basal conditions.

Acute inflammation is one of the features of LPC-induced demyelination (Blanchard et al., 2013; Watanabe et al., 2002).

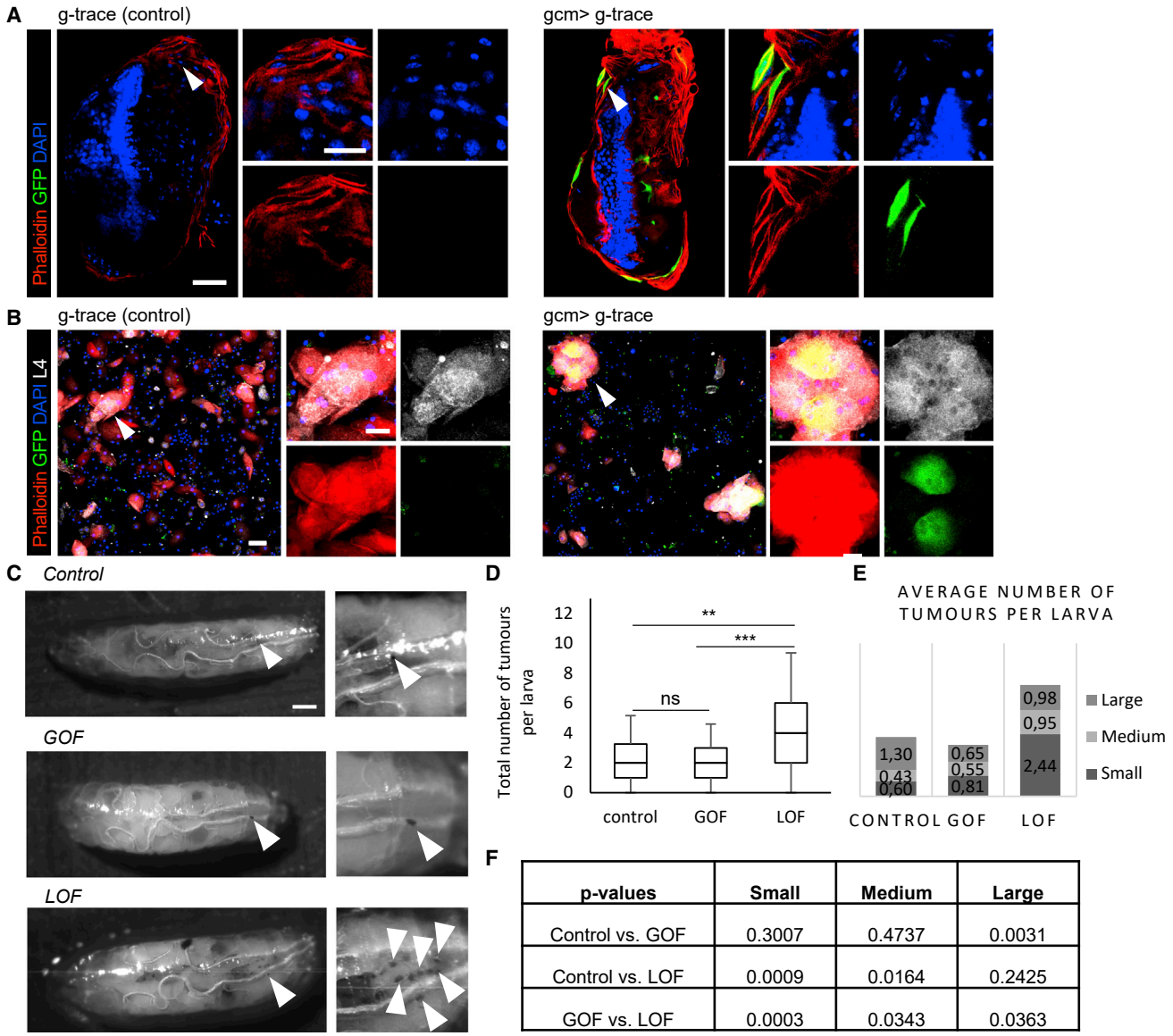

F

p-values	Small	Medium	Large
Control vs. GOF	0.3007	0.4737	0.0031
Control vs. LOF	0.0009	0.0164	0.2425
GOF vs. LOF	0.0003	0.0343	0.0363

Figure 6. Acute inflammation induces *gcm* expression

(A and B) Tracing of *gcm* expression in activated hemocytes (lamellocytes) surrounding the wasp embryo (nuclei visible with DAPI [blue]) that was dissected out of the larva (A) and in lamellocytes in the circulating hemolymph (B). Phalloidin (red), *gcm > g-trace* (green), lamellocyte marker L4 (gray), and DAPI (blue). n = 3. Scale bar for enlarged picture: 50 μm; for magnification: 10 μm.

(C) Bright-field images of infested larvae for the control (*w;hml ΔGal4/+;tubGal80TS/+*), GOF (*w;hml ΔGal4/+;tubGal80TS/UASTgcmF18A*), and LOF (*w;hml ΔGal4/+;*
tubGal80TS/UASgcmRNAi) genotypes. The arrowheads indicate the small-size tumors. Scale bar: 100 μm.

(D) Quantification of the total number of tumors per larva.

(E and F) Quantification of the average number of tumors per larva according to their size and the p values (F). *p < 0.05, **p < 0.01, ****p < 0.0001, and ns, not significant. n = 10–25 larvae per trial, 3 trials.

The fact that the mGcm2 protein is present in few CD45$^+$ immune cells after acute demyelination induced by LPC injection indicates that mGcm2 expression is restricted to a subset of inflammatory cells. Moreover, we provide compelling evidence that mGcm2 expression is induced in a subset of microglia/macrophages, specifically in demyelinated lesions, using double RNA ISH for *mGcm2* and *Cx3cr1*. Our data, gained using the mGcm2 icKO, specifically in microglia/macrophages, clearly indicate that mGcm2 favors an anti-inflammatory M2 state and could therefore promote indirectly myelin regeneration and repair by modulating OPC differentiation after acute demyelination (Miron et al., 2013). hGCM2 expression is also detected in a small fraction of MHC class II/CD68 double-positive cells located specifically in active lesions and in the active rim of

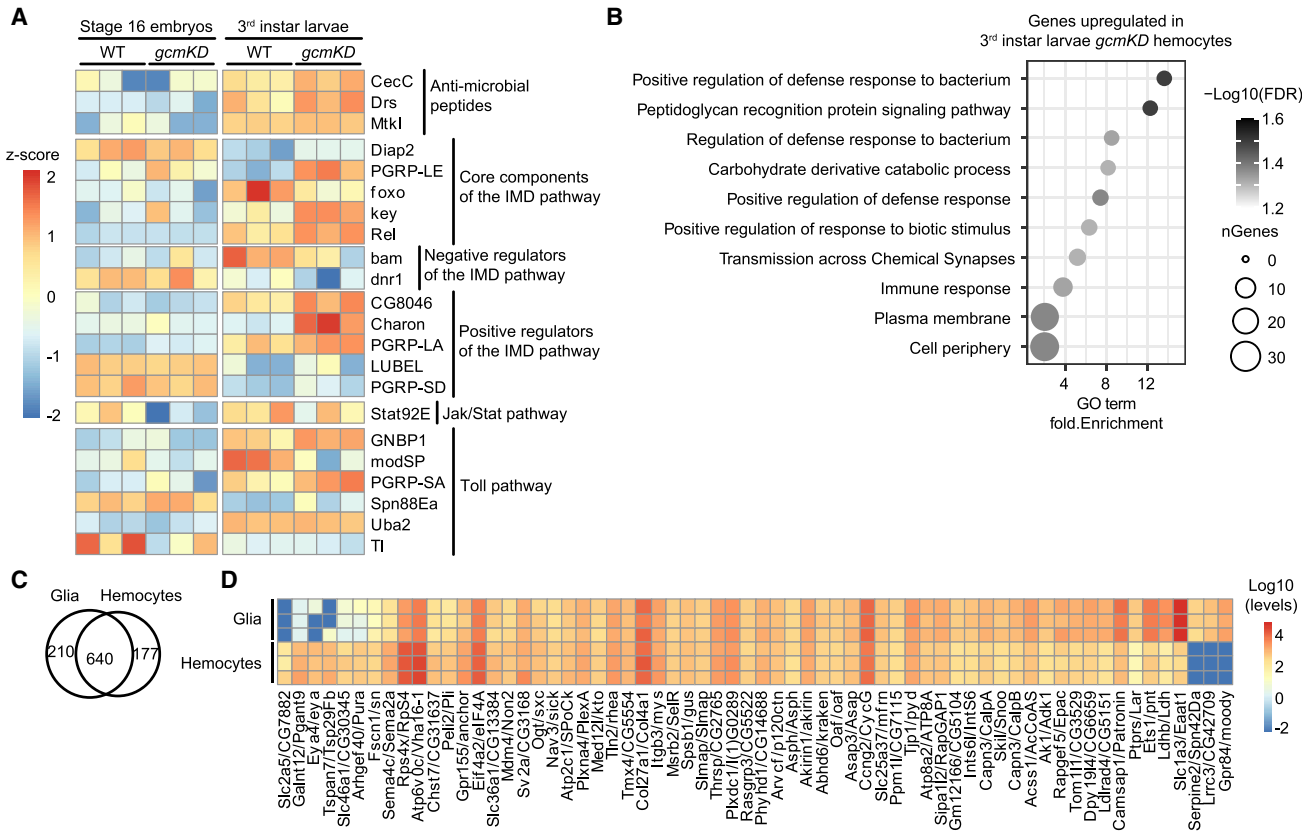

Figure 7. RNA-seq data from microglia and from fly hemocytes and glia

(A) Heatmap from RNA-seq data showing differentially expressed genes in hemocytes from late embryos (embryonic day 16 [E16]) and wandering third-instar larvae.

(B) GO term analysis of the genes upregulated in *gcmKD* hemocytes from wandering third-instar larvae.

(C) Diagram representing the number of microglial markers upregulated in glia or hemocytes or expressed in both tissues at similar levels. The genes upregulated in a specific tissue present an expression fold difference above 2 and a $p < 0.05$ (determined using DESeq2).

(D) Heatmap representing the expression levels (log10 scale) of the orthologs of microglial markers in *Drosophila* adult hemocytes and glia. The markers presenting the strongest expressions (>500 reads) were selected. The expression levels were retrieved from the datasets GEO: GSE79488 (adult hemocytes) and GEO: GSE142788 (adult glia) and analyzed using DESeq2.

chronic active lesions of MS, further supporting a conserved function of Gcm2 in microglial lineage cells in humans. This emerging anti-inflammatory role of Gcm2 may open therapeutic interventions, targeting this transcription factor in demyelinating diseases.

Our data explain what was considered as a longstanding conundrum. The fly *gcm* gene was initially described for its developmental role in glia and hemocytes (Bernardoni et al., 1997; Vincent et al., 1996). Surprisingly, while the genes necessary for neuronal differentiation are functionally conserved in evolution, the orthologs of Gcm are neither expressed nor required in the differentiation of vertebrate glia (Mao et al., 2012). The gliogenic pathway does not seem to be evolutionarily conserved, in line with the hypothesis that glia may have evolved several times, adapting to the needs of the organism (Hartline, 2011). The glia of simple organisms play a neural role, as they control axon ensheathment and synapse activity and insulate the brain through the BBB. In addition, they act as the resident immune cells of the nervous system. In complex organisms, the role of the brain-resident immune cells is taken by another cell type, the microglia, a myeloid population that infiltrates the nervous system before the BBB is formed. This division of labor guarantees a better and more targeted response to inflammatory challenges. We speculate that the hemocytes of simple, fast-developing animals migrate along the nervous system to remove dying cells, but as the BBB forms, they are excluded from the neural tissue, with the immune function being taken up by the glial cells. According to this hypothesis, we should find orthologs of microglial markers being expressed in fly hemocytes as well as glia. A recent and elegant study characterized the microglia transcriptional programs across 10 species spanning more than 450 million years of evolution (Geirsdottir et al., 2019). By using these data with the published RNA sequencing (RNA-seq) data from adult fly hemocytes and glia, we created a heatmap of the microglia orthologs in *Drosophila* (Nazario-Toole et al., 2018; Ozel et al., 2021). These orthologs are mostly shared between the two fly cell populations (Figures 7C and 7D). One microglial gene whose ortholog

is shared by hemocytes and glia is Peli2, a member of E3 ubiquitin ligases controlling the Toll signaling pathway (Schauvliege et al., 2007). The *Pellino* (*Pli*) fly gene antagonizes Toll-mediated innate immune signaling by controlling MyD88 turnover in macrophages. Future studies will determine whether the pathway is also conserved in glia. In addition to the shared genes, some are specific to glia (*spn42Da*, *moody*, *CG42709*) or hemocytes (*CG7882*, *pgant9*, *eya*, and *CG30345*). Interestingly, *moody* is one of the most known markers of the *Drosophila* BBB glia, and its ortholog in mammals (*Gpr84*) is a well-known pro-inflammatory maker that is highly upregulated in microglia upon nerve injury (Wei et al., 2017). Revisiting the role of *moody* during neuroinflammation could shed light onto the function of this gene in both species. As a corollary of the above and based on multiple evidence, we propose that *repo* constitutes the bona fide fly gliogenic gene. Accordingly, Repo misexpression in the mesoderm suppresses hematopoiesis, and its lack triggers the expression of hemocyte markers in the nervous system (Trebuchet et al., 2019). We speculate that the Gcm pathway has an ancestral, conserved role in immunity and has been co-opted in the differentiation of fly glia. One of the future challenges will be to characterize the Gcm^{+} cells associated with the aged brain.

Together with the inhibitory role of Gcm on the JAK/STAT pathway and the increased response to wasp infestation, which relies on the Toll cascade, the present data strongly suggest that Gcm controls a variety of inflammatory conditions (Bazzi et al., 2018). The present data come to add other perspectives. In addition to an effect of Gcm on priming during development (Bazzi et al., 2018), its *de novo* expression in activated hemocytes also contributes to counteract the inflammatory state. This is in line with the transcriptomic data of the *gcmKD* animals, which confirm the induction of the JAK/STAT pathway observed *in vivo* and extend the inhibitory role of Gcm to other pathways such as immune deficiency (IMD). We hypothesize that the induction of the Gcm cascade reduces the intensity of the inflammatory response and hence has a protective function. This hypothesis is corroborated by recent data obtained in other organisms. A peculiar macrophage population called pigment cells is present in the sea urchin (Perillo et al., 2020). Such cells are involved in the immune defense by the production of a pigment that has anti-microbial properties. Morpholino anti-sense oligonucleotides for *Spgcm* (*gcmMO*) injection showed that *gcmMO* animals are less resistant to challenging environmental conditions, portrayed by a decreased survival rate compared with the control (Davidson et al., 2002; Ransick and Davidson, 2006, 2012). A recent study showed that a *gcm* ortholog is also expressed in glia-like cells of the freshwater crayfish (*Pacifastacus leniusculus*) upon an acute inflammatory response (Junkunlo et al., 2020). Moreover, the expression of a planaria *gcm* ortholog was found to be induced upon regeneration in a subset of cells close to the wound; its silencing has no effect in homeostatic conditions but impairs neoblast repopulation upon wounding (Umesono and Agata, 2009). These studies suggest an evolutionarily conserved mechanism.

In sum, we report an anti-inflammatory transcriptional cascade that is conserved from flies to humans. Given the strong potential of transcription factors in coordinating the expression of several genes and the scarce number of known transcription factors with a similar function, this work represents a major contribution to understand the molecular mechanisms controlling the inflammatory response. It also lays the ground for studying therapeutical targets for diseases where the inflammatory response needs to be contained.

Limitations of this study

Our study uncovers an anti-inflammatory cascade, conserved from flies to mammals. There are two potential caveats of the work. We show that mGcm2 is present in microglia/macrophages during chronic and acute inflammation. A comparative RNA-seq analysis could shed light on the mGcm2 pathway and highlight its targets, but given the relatively low levels of mGcm2 expression, this may not be sufficiently informative upon using the current techniques. Second, the *gcm*-expressing cells in the old *Drosophila* brains are not positive for either P1 or Hemese, which are two fairly broad hemocyte markers. In addition, they represent a small subpopulation of hemocytes that we cannot identify with independent markers. Single-cell RNA-seq data from the adult hemocytes will help understanding the role and mode of action of Gcm, but only if performed with highly sensitive techniques.

STAR★METHODS

Detailed methods are provided in the online version of this paper and include the following:

- KEY RESOURCES TABLE
- RESOURCE AVAILABILITY
  - Lead contact
  - Materials availability
  - Data and code availability
- EXPERIMENTAL MODEL AND SUBJECT DETAILS
  - Mouse lines
  - MS tissue samples
- METHOD DETAILS
  - Genotyping
  - Tamoxifen treatment
  - LPC-induced demyelination of the mouse spinal cord
  - P1 primary CNS cultures
  - Tissue dissections
  - Immunolabelling in mouse samples
  - Oil red O staining
  - MS tissue samples
  - Quantitative RT-PCR analysis
  - RNAscope multiplex assay
  - Imaging
  - Transcriptome analysis of gcmKD haemocytes from *Drosophila* embryos and larvae
  - Expression profile of the microglial markers in adult *Drosophila* haemocytes and glia
  - Tracing *gcm* expression
  - Wasp infestation assays
  - Adult CNS dissection
- QUANTIFICATION AND STATISTICAL ANALYSIS
  - Image analysis
  - Statistical analysis

SUPPLEMENTAL INFORMATION

Supplemental information can be found online at https://doi.org/10.1016/j.celrep.2022.111506.

ACKNOWLEDGMENTS

We thank the Imaging Center of the IGBMC for technical assistance, as well as the Mouse Clinic (ICS) for producing the mGcm2flox/flox strain. We also thank the ICM mouse facility (ICMice) and the ICM histology (Histomics) and cellular imaging (ICM-Quant) facilities. We are grateful to Francois-Xavier Lejeune from the ICM Data Analysis Core (DAC) for biostatistics analysis. A.P. was supported by the ARSEP Foundation and a grant from Laboratoires d'excellence (LabEx INRT), S.M. by CEFIPRA and the FRM Foundations, and Y.Y. by the ARSEP foundation. R.P. was funded by the ARSEP Foundation and NeurATRIS. This work was supported by INSERM, CNRS, UDS, Ligue Régionale contre le Cancer, Hôpital de Strasbourg, ARC, CEFIPRA, ANR grants, the CNRS/University LIA Calim, The French MS Foundation ARSEP, and the Investissements d'Avenir ANR-10-IAIHU-06 (IHU-A-ICM) and ANR-11-INBS-0011 (NeurATRIS). The IGBMC was also supported by a French state fund through the ANR labex. We are grateful to the UK Multiple Sclerosis Tissue Bank, funded by the Multiple Sclerosis Society of Great Britain and Northern Ireland (registered charity 207495) for providing MS and control brain tissue samples (registered charity 207495) and to C. Linnington and I. Ando for providing antibodies.

AUTHOR CONTRIBUTIONS

A.P., S.M., P.B.C., R.P., B.N.-O., and A.G. designed the experiments and cowrote the manuscript. A.P., S.M., C.R., and R.P. performed the experiments in mice. R.P. performed the experiments in humans. S.M. and A.P. performed the assays in *D. melanogaster*. Y.Y. was responsible for the mGcm2flox/flox production. P.B.C. analyzed the RNA-seq data.

DECLARATION OF INTERESTS

The authors declare no competing interests.

Received: July 14, 2022
Revised: August 19, 2022
Accepted: September 22, 2022
Published: October 11, 2022

REFERENCES

Afgan, E., Baker, D., Batut, B., van den Beek, M., Bouvier, D., Cech, M., Chilton, J., Clements, D., Coraor, N., Grüning, B.A., et al. (2018). The Galaxy platform for accessible, reproducible and collaborative biomedical analyses: 2018 update. Nucleic Acids Res. *46*, W537–W544.

Anders, S., Pyl, P.T., and Huber, W. (2015). HTSeq–a Python framework to work with high-throughput sequencing data. Bioinformatics *31*, 166–169.

Bazzi, W., Cattenoz, P.B., Delaporte, C., Dasari, V., Sakr, R., Yuasa, Y., and Giangrande, A. (2018). Embryonic hematopoiesis modulates the inflammatory response and larval hematopoiesis in Drosophila. Elife *7*, e34890.

Bernardoni, R., Vivancos, V., and Giangrande, A. (1997). glide/gcm is expressed and required in the scavenger cell lineage. Dev. Biol. *191*, 118–130.

Blanchard, B., Heurtaux, T., Garcia, C., Moll, N.M., Caillava, C., Grandbarbe, L., Klosptein, A., Kerninon, C., Frah, M., Coowar, D., et al. (2013). Tocopherol derivative TFA-12 promotes myelin repair in experimental models of multiple sclerosis. J. Neurosci. *33*, 11633–11642.

Bohatschek, M., Kloss, C.U., Kalla, R., and Raivich, G. (2001). In vitro model of microglial deramification: ramified microglia transform into amoeboid phagocytes following addition of brain cell membranes to microglia-astrocyte cocultures. J. Neurosci. Res. *64*, 508–522.

Buchmann, K. (2014). Evolution of innate immunity: clues from invertebrates via fish to mammals. Front. Immunol. *5*, 459.

Butovsky, O., Jedrychowski, M.P., Moore, C.S., Cialic, R., Lanser, A.J., Gabriely, G., Koeglsperger, T., Dake, B., Wu, P.M., Doykan, C.E., et al. (2014). Identification of a unique TGF-beta-dependent molecular and functional signature in microglia. Nat. Neurosci. *17*, 131–143.

Cattenoz, P.B., and Giangrande, A. (2015). New insights in the clockwork mechanism regulating lineage specification: lessons from the Drosophila nervous system. Dev. Dynam. *244*, 332–341.

Cattenoz, P.B., Monticelli, S., Pavlidaki, A., and Giangrande, A. (2021). Toward a consensus in the repertoire of haemocytes identified in Drosophila. Front. Cell Dev. Biol. *9*, 643712.

Cattenoz, P.B., Popkova, A., Southall, T.D., Aiello, G., Brand, A.H., and Giangrande, A. (2016). Functional conservation of the glide/gcm regulatory network controlling glia, haemocyte, and tendon cell differentiation in Drosophila. Genetics *202*, 191–219.

Cattenoz, P.B., Sakr, R., Pavlidaki, A., Delaporte, C., Riba, A., Molina, N., Hariharan, N., Mukherjee, T., and Giangrande, A. (2020). Temporal specificity and heterogeneity of Drosophila immune cells. The EMBO journal *39*, e104486.

Cengiz, P., Zafer, D., Chandrashekhar, J.H., Chanana, V., Bogost, J., Waldman, A., Novak, B., Kintner, D.B., and Ferrazzano, P.A. (2019). Developmental differences in microglia morphology and gene expression during normal brain development and in response to hypoxia-ischemia. Neurochem. Int. *127*, 137–147.

Chiang, M.H., Liang, F.Y., Chen, C.P., Chang, C.W., Cheong, M.L., Wang, L.J., Liang, C.Y., Lin, F.Y., Chou, C.C., and Chen, H. (2009). Mechanism of hypoxia-induced GCM1 degradation: implications for the pathogenesis of preeclampsia. J. Biol. Chem. *284*, 17411–17419.

Clark, R.I., Woodcock, K.J., Geissmann, F., Trouillet, C., and Dionne, M.S. (2011). Multiple TGF-beta superfamily signals modulate the adult Drosophila immune response. Curr. Biol. *21*, 1672–1677.

Colton, C.A. (2009). Heterogeneity of microglial activation in the innate immune response in the brain. J. Neuroimmune Pharmacol. *4*, 399–418.

Conde, J.R., and Streit, W.J. (2006). Microglia in the aging brain. J. Neuropathol. Exp. Neurol. *65*, 199–203.

Damani, M.R., Zhao, L., Fontainhas, A.M., Amaral, J., Fariss, R.N., and Wong, W.T. (2011). Age-related alterations in the dynamic behavior of microglia. Aging Cell *10*, 263–276.

Davidson, E.H., Rast, J.P., Oliveri, P., Ransick, A., Calestani, C., Yuh, C.H., Minokawa, T., Amore, G., Hinman, V., Arenas-Mena, C., et al. (2002). A genomic regulatory network for development. Science *295*, 1669–1678.

Davie, K., Janssens, J., Koldere, D., De Waegeneer, M., Pech, U., Kreft, Ł., Aibar, S., Makhzami, S., Christiaens, V., Bravo González-Blas, C., et al. (2018). A single-cell transcriptome atlas of the aging Drosophila brain. Cell *174*, 982–998.e20.

Denes, A., Coutts, G., Lénárt, N., Cruickshank, S.M., Pelegrin, P., Skinner, J., Rothwell, N., Allan, S.M., and Brough, D. (2015). AIM2 and NLRC4 inflammasomes contribute with ASC to acute brain injury independently of NLRP3. Proc. Natl. Acad. Sci. USA. *112*, 4050–4055.

Dunin-Horkawicz, S., Kopec, K.O., and Lupas, A.N. (2014). Prokaryotic ancestry of eukaryotic protein networks mediating innate immunity and apoptosis. J. Mol. Biol. *426*, 1568–1582.

Evans, C.J., Olson, J.M., Ngo, K.T., Kim, E., Lee, N.E., Kuoy, E., Patananan, A.N., Sitz, D., Tran, P., Do, M.T., et al. (2009). G-TRACE: rapid Gal4-based cell lineage analysis in Drosophila. Nat. Methods *6*, 603–605.

Fabian, D.K., Fuentealba, M., Dönertaş, H.M., Partridge, L., and Thornton, J.M. (2021). Functional conservation in genes and pathways linking ageing and immunity. Immun. Ageing *18*, 23.

Fadok, V.A., Bratton, D.L., Konowal, A., Freed, P.W., Westcott, J.Y., and Henson, P.M. (1998). Macrophages that have ingested apoptotic cells in vitro inhibit proinflammatory cytokine production through autocrine/paracrine

mechanisms involving TGF-beta, PGE2, and PAF. J. Clin. Invest. *101*, 890–898.

Flici, H., Cattenoz, P.B., Komonyi, O., Laneve, P., Erkosar, B., Karatas, O.F., Reichert, H., Berzsenyi, S., and Giangrande, A. (2014). Interlocked loops trigger lineage specification and stable fates in the Drosophila nervous system. Nat. Commun. *5*, 4484.

Ge, S.X., Jung, D., and Yao, R. (2020). ShinyGO: a graphical gene-set enrichment tool for animals and plants. Bioinformatics *36*, 2628–2629.

Geirsdottir, L., David, E., Keren-Shaul, H., Weiner, A., Bohlen, S.C., Neuber, J., Balic, A., Giladi, A., Sheban, F., Dutertre, C.A., et al. (2019). Cross-species single-cell analysis reveals divergence of the primate microglia program. Cell *179*, 1609–1622.e16.

Gober, R., Ardalan, M., Shiadeh, S.M.J., Duque, L., Garamszegi, S.P., Ascona, M., Barreda, A., Sun, X., Mallard, C., and Vontell, R.T. (2022). Microglia activation in postmortem brains with schizophrenia demonstrates distinct morphological changes between brain regions. Brain Pathol. *32*, e13003.

Gordon, J., Bennett, A.R., Blackburn, C.C., and Manley, N.R. (2001). Gcm2 and Foxn1 mark early parathyroid- and thymus-specific domains in the developing third pharyngeal pouch. Mech. Dev. *103*, 141–143.

Gordon, S. (2003). Alternative activation of macrophages. Nat. Rev. Immunol. *3*, 23–35.

Günther, T., Chen, Z.F., Kim, J., Priemel, M., Rueger, J.M., Amling, M., Moseley, J.M., Martin, T.J., Anderson, D.J., and Karsenty, G. (2000). Genetic ablation of parathyroid glands reveals another source of parathyroid hormone. Nature *406*, 199–203.

Hartline, D.K. (2011). The evolutionary origins of glia. Glia *59*, 1215–1236.

Heindl, S., Gesierich, B., Benakis, C., Llovera, G., Duering, M., and Liesz, A. (2018). Automated morphological analysis of microglia after stroke. Front. Cell. Neurosci. *12*, 106.

Jacques, C., Soustelle, L., Nagy, I., Diebold, C., and Giangrande, A. (2009). A novel role of the glial fate determinant glial cells missing in hematopoiesis. Int. J. Dev. Biol. *53*, 1013–1022.

Junkunlo, K., Söderhäll, K., and Söderhäll, I. (2020). A transcription factor glial cell missing (Gcm) in the freshwater crayfish Pacifastacus leniusculus. Dev. Comp. Immunol. *113*, 103782.

Kim, J., Jones, B.W., Zock, C., Chen, Z., Wang, H., Goodman, C.S., and Anderson, D.J. (1998). Isolation and characterization of mammalian homologs of the Drosophila gene glial cells missing. Proc. Natl. Acad. Sci. USA. *95*, 12364–12369.

Kim-Jo, C., Gatti, J.L., and Poirié, M. (2019). Drosophila cellular immunity against parasitoid wasps: a complex and time-dependent process. Front. Physiol. *10*, 603.

Lan, W., Liu, S., Zhao, L., and Su, Y. (2020). Regulation of Drosophila hematopoiesis in lymph gland: from a developmental signaling point of view. Int. J. Mol. Sci. *21*, E5246.

Leyh, J., Paeschke, S., Mages, B., Michalski, D., Nowicki, M., Bechmann, I., and Winter, K. (2021). Classification of microglial morphological phenotypes using machine learning. Front. Cell. Neurosci. *15*, 701673.

Lisi, L., Ciotti, G.M.P., Braun, D., Kalinin, S., Currò, D., Dello Russo, C., Coli, A., Mangiola, A., Anile, C., Feinstein, D.L., and Navarra, P. (2017). Expression of iNOS, CD163 and ARG-1 taken as M1 and M2 markers of microglial polarization in human glioblastoma and the surrounding normal parenchyma. Neurosci. Lett. *645*, 106–112.

López-Otín, C., Blasco, M.A., Partridge, L., Serrano, M., and Kroemer, G. (2013). The hallmarks of aging. Cell *153*, 1194–1217.

Mao, H., Lv, Z., and Ho, M.S. (2012). Gcm proteins function in the developing nervous system. Dev. Biol. *370*, 63–70.

Michell-Robinson, M.A., Touil, H., Healy, L.M., Owen, D.R., Durafourt, B.A., Bar-Or, A., Antel, J.P., and Moore, C.S. (2015). Roles of microglia in brain development, tissue maintenance and repair. Brain *138*, 1138–1159.

Miron, V.E., Boyd, A., Zhao, J.W., Yuen, T.J., Ruckh, J.M., Shadrach, J.L., van Wijngaarden, P., Wagers, A.J., Williams, A., Franklin, R.J.M., and Ffrench-Constant, C. (2013). M2 microglia and macrophages drive oligodendrocyte differentiation during CNS remyelination. Nat. Neurosci. *16*, 1211–1218.

Nait-Oumesmar, B., Copperman, A.B., and Lazzarini, R.A. (2000). Placental expression and chromosomal localization of the human Gcm 1 gene. J. Histochem. Cytochem. *48*, 915–922.

Nait-Oumesmar, B., Picard-Riera, N., Kerninon, C., Decker, L., Seilhean, D., Höglinger, G.U., Hirsch, E.C., Reynolds, R., and Baron-Van Evercooren, A. (2007). Activation of the subventricular zone in multiple sclerosis: evidence for early glial progenitors. Proc. Natl. Acad. Sci. USA. *104*, 4694–4699.

Nazario-Toole, A.E., Robalino, J., Okrah, K., Corrada-Bravo, H., Mount, S.M., and Wu, L.P. (2018). The splicing factor RNA-binding fox protein 1 mediates the cellular immune response in Drosophila melanogaster. J. Immunol. *201*, 1154–1164.

Ovanesov, M.V., Sauder, C., Rubin, S.A., Richt, J., Nath, A., Carbone, K.M., and Pletnikov, M.V. (2006). Activation of microglia by borna disease virus infection: in vitro study. J. Virol. *80*, 12141–12148.

Özel, M.N., Simon, F., Jafari, S., Holguera, I., Chen, Y.C., Benhra, N., El-Danaf, R.N., Kapuralin, K., Malin, J.A., Konstantinides, N., and Desplan, C. (2021). Neuronal diversity and convergence in a visual system developmental atlas. Nature *589*, 88–95.

Parkhurst, C.N., Yang, G., Ninan, I., Savas, J.N., Yates, J.R., 3rd, Lafaille, J.J., Hempstead, B.L., Littman, D.R., and Gan, W.B. (2013). Microglia promote learning-dependent synapse formation through brain-derived neurotrophic factor. Cell *155*, 1596–1609.

Peissig, K., Condie, B.G., and Manley, N.R. (2018). Embryology of the parathyroid glands. Endocrinol. Metab. Clin. North Am. *47*, 733–742.

Perillo, M., Oulhen, N., Foster, S., Spurrell, M., Calestani, C., and Wessel, G. (2020). Regulation of dynamic pigment cell states at single-cell resolution. Elife *9*, e60388.

Perry, V.H., Matyszak, M.K., and Fearn, S. (1993). Altered antigen expression of microglia in the aged rodent CNS. Glia *7*, 60–67.

Rangaraju, S., Raza, S.A., Li, N.X., Betarbet, R., Dammer, E.B., Duong, D., Lah, J.J., Seyfried, N.T., and Levey, A.I. (2018). Differential phagocytic properties of CD45(low) microglia and CD45(high) brain mononuclear phagocytes-activation and age-related effects. Front. Immunol. *9*, 405.

Ransick, A., and Davidson, E.H. (2006). cis-regulatory processing of Notch signaling input to the sea urchin glial cells missing gene during mesoderm specification. Dev. Biol. *297*, 587–602.

Ransick, A., and Davidson, E.H. (2012). Cis-regulatory logic driving glial cells missing: self-sustaining circuitry in later embryogenesis. Dev. Biol. *364*, 259–267.

Ransohoff, R.M. (2016). How neuroinflammation contributes to neurodegeneration. Science *353*, 777–783.

Rodríguez, J.J., Olabarria, M., Chvatal, A., and Verkhratsky, A. (2009). Astroglia in dementia and Alzheimer's disease. Cell Death Differ. *16*, 378–385.

Schauvliege, R., Janssens, S., and Beyaert, R. (2007). Pellino proteins: novel players in TLR and IL-1R signalling. J. Cell Mol. Med. *11*, 453–461.

Soustelle, L., and Giangrande, A. (2007). Novel gcm-dependent lineages in the postembryonic nervous system of Drosophila melanogaster. Dev. Dynam. *236*, 2101–2108.

Spittau, B. (2017). Aging microglia-phenotypes, functions and implications for age-related neurodegenerative diseases. Front. Aging Neurosci. *9*, 194.

Thored, P., Heldmann, U., Gomes-Leal, W., Gisler, R., Darsalia, V., Taneera, J., Nygren, J.M., Jacobsen, S.E.W., Ekdahl, C.T., Kokaia, Z., and Lindvall, O. (2009). Long-term accumulation of microglia with proneurogenic phenotype concomitant with persistent neurogenesis in adult subventricular zone after stroke. Glia *57*, 835–849.

Trébuchet, G., Cattenoz, P.B., Zsámboki, J., Mazaud, D., Siekhaus, D.E., Fanto, M., and Giangrande, A. (2019). The repo homeodomain transcription

factor suppresses hematopoiesis in Drosophila and preserves the glial fate. J. Neurosci. *39*, 238–255.

Tremblay, M.È., Zettel, M.L., Ison, J.R., Allen, P.D., and Majewska, A.K. (2012). Effects of aging and sensory loss on glial cells in mouse visual and auditory cortices. Glia *60*, 541–558.

Umesono, Y., and Agata, K. (2009). Evolution and regeneration of the planarian central nervous system. Dev. Growth Differ. *51*, 185–195.

Vincent, S., Vonesch, J.L., and Giangrande, A. (1996). Glide directs glial fate commitment and cell fate switch between neurones and glia. Development *122*, 131–139.

Watanabe, T., Pakala, R., Katagiri, T., and Benedict, C.R. (2002). Lysophosphatidylcholine is a major contributor to the synergistic effect of mildly oxidized low-density lipoprotein with endothelin-1 on vascular smooth muscle cell proliferation. J. Cardiovasc. Pharmacol. *39*, 449–459.

Wei, L., Tokizane, K., Konishi, H., Yu, H.R., and Kiyama, H. (2017). Agonists for G-protein-coupled receptor 84 (GPR84) alter cellular morphology and motility but do not induce pro-inflammatory responses in microglia. J. Neuroinflammation *14*, 198.

Winkler, B., Funke, D., Benmimoun, B., Spéder, P., Rey, S., Logan, M.A., and Klämbt, C. (2021). Brain inflammation triggers macrophage invasion across the blood-brain barrier in Drosophila during pupal stages. Sci. Adv. *7*, eabh0050.

STAR★METHODS

KEY RESOURCES TABLE

REAGENT or RESOURCE	SOURCE	IDENTIFIER
Antibodies		
anti-Arginase1	Santa Cruz Biotechnology	sc-271430; RRID:AB_10648473
anti-CD11b	Bio-Rad	MCA-74G; RRID:AB_321293
anti-CD45	Bio-Rad	MCD-4500; RRID:AB_1476133
anti-CD68	Bio-Rad	MCA-1957; RRID:AB_322219
anti-F4/80	Bio-Rad	MCA-497; RRID:AB_2335599
anti-Gcm1	B. Nait-Oumesmar	N/A
anti-Gcm2	Abcam	ab201170; RRID:AB_2891136
anti-Iba1	Wako	01919741; RRID:AB_839504
anti-iNOS	Abcam	ab210823
anti-GFAP	PCN	N/A
anti-NeuN	Abcam	ab279296
anti-Casp3	Cell signalling technology	mAb #9664
anti-MOG	C. Linnington, University of Glasgow	clone C18C5
anti-Olig2	Merck	AB9610; RRID:AB_570666
anti-APC	Merck	OP80; RRID:AB_2057371
anti-HLA	Abcam	CR3/43
anti-Repo	DSHB	8D12; RRID:AB_528448
anti-Elav	DSHB	7E8A10; RRID:AB_528218
anti-Hemese	I. Ando	N/A
anti-L4	I. Ando	N/A
anti-GFP	Jackson Immuno Research	703095155; RRID:AB_2340356
anti-mouse-Cy3	Jackson Immuno Research	715-165-151
anti-rabbit-Cy3	Jackson Immuno Research	711-165-152
anti-rat-Cy3	Jackson Immuno Research	112-165-167; RRID:AB_2338251
anti-mouse-Alexa647	Jackson Immuno Research	115-605-166; RRID:AB_2338914
anti-rabbit-Cy5	Jackson Immuno Research	111-175-144; RRID:AB_2338013
anti-rat-Cy5	Jackson Immuno Research	112-175-144
anti-chicken-FITC	Invitrogen	A11039; RRID:AB_2534096
anti-rat-Alexa568	Invitrogen	A11077; RRID:AB_2534121
anti-rat-Alexa488	Invitrogen	A21208; RRID:AB_141709
anti-rat-Alexa647	Abcam	AB150155; RRID:AB_2813835
anti-rabbit-Alexa568	Invitrogen	A10042; RRID:AB_2534017
anti-mouse-Alexa488	Southern Biotech	1070-02; RRID:AB_2794409
anti-mouse-Alexa488	Invitrogen	A21202; RRID:AB_141607
anti-mouse-FITC	Invitrogen	A21141; RRID:AB_141626
Biological samples		
Human MS patient tissues	MS tissue bank, Imperial College, London	https://www.imperial.ac.uk/medicine/multiple-sclerosis-and-parkinsons-tissue-bank
Chemicals, peptides, and recombinant proteins		
DAPI	Sigma-Aldrich	#D9542
4 % PFA	Electron Microscopy Sciences	50-980-487
Aqua Poly/Mount	Polysciences	18606-20

(*Continued on next page*)

Continued

REAGENT or RESOURCE	SOURCE	IDENTIFIER
O.C.T.	Thermo Fisher	12678646
avidin–biotin–peroxidase (ABC) complex	Vector Laboratories	AK-5000
3,3′ diaminobenzidine tetrahydrochloride (DAB)	Sigma–Aldrich	D5637-1G
Oil Red O (ORO)	Sigma–Aldrich	O0625
Tyramide dye fluorophores (Cy3, Cy5)	Aykoya	NEL744001KT, NEL745001KT
Opal fluorophores (Opal 520, Opal 570, Opal 690,)	Aykoya	FP1487001KT, FP1488001KT, FP1497001KT
RNAscope Multiplex TSA dilution buffer	Aykoya	ARD1001EA
Tri-reagent	Sigma-Aldrich	93289
Vectashield mounting medium	Vector Laboratories	H-1000-10
Critical commercial assays		
RNeasy Mini Kit	Qiagen	#74104
High-capacity cDNA reverse transcription kit with RNase inhibitor	Applied Biosystem	#4374967
TaqMan Fast Advanced Master Mix	Thermo Fisher	#4444556
RNAscope Multiplex TSA dilution buffer	ACDbio	322381
RNAscope Multiplex TSA dilution buffer	ACDbio	323110
SMARTer	Takara	634940
Deposited data		
Bulk RNAseq data from *Drosophila* haemocytes	www.ebi.ac.uk/arrayexpress	E-MTAB-8702
Experimental models: Organisms/strains		
Mouse: Cx3cr1-Cre	TAAM Orléans	N/A
Mouse: mGcm2flox/flox	ICS	N/A
Mouse	JAX	stock #021160
Drosophila: *srp(hemo)Gal4/+;UAS-RFP/+*	Build in this paper by combining srp(hemo) Gal (RRID:BDSC_ 78565) and UAS-RFP (RRID:BDSC_8547).	RRID:BDSC_78565 RRID:BDSC_8547
Drosophila: *UAS-gcm-RNAi*	BDRC	#31519
Drosoohila: *UAS-FLP/+;act5c-FRT,y+,FRT-Gal4, UASmCD8GFP/CyoGFP,tubulinGal80TS; UAS-FLP,Ubi-p63E(FRT.STOP)Stinger/TM6TBHu*	in this paper	N/A
Drosoohila: *gcmGal4,tubulinGal80TS/ CyoGFP; 6KbgcmGal4*	in this paper	N/A
Drosophila: *w[1118]*	BDRC	#3605
Drosophila:y[1]v[1];P{y[+t7.7] v[+t1.8]=TRiP.HM05124}attP2	BDRC	#28913
Drosophila: *UAS-gcm (F18A (one transgene)*	Flici et al., 2014	N/A
Leptopilina boulardi	M. Crozatier	N/A
Oligonoucleotides		
Table S2	in this paper	N/A
Software and algorithms		
Image J	in this paper	https://imagej.nih.gov/ij/
Imaris	in this paper	https://imaris.oxinst.com/
Visiopharm	in this paper	https://visiopharm.com/

(*Continued on next page*)

Continued

REAGENT or RESOURCE	SOURCE	IDENTIFIER
ggplot2	https://ggplot2.tidyverse.org/	RRID:SCR_014601
Pheatmap	https://www.rdocumentation.org/packages/pheatmap/versions/1.0.12/topics/pheatmap	RRID:SCR_016418
ShinyGO 0.76 65	http://bioinformatics.sdstate.edu/go/	RRID:SCR_019213
DESeq2	https://bioconductor.org/packages/release/bioc/html/DESeq2.html	RRID:SCR_015687
HTseq-Count	https://htseq.readthedocs.io/en/master/	RRID:SCR_011867
GraphPad Prism version 9.3.1		

RESOURCE AVAILABILITY

Lead contact

Further information and requests for reagents should be directed to and will be fulfilled by corresponding authors Brahim Nait-Oumesmar (brahim.nait_oumesmar@upmc.fr) and Angela Giangrande (angela@igbmc.fr). The lead contact is Angela Giangrande.

Materials availability

This study did not generate new unique reagents.

Data and code availability

The raw sequencing data generated in this study have been deposited in ArrayExpress under the accession number listed in the key resources table.

This paper does not report original code.

Any additional information required to reanalyze the data reported in this paper is available from the lead contact upon request.

EXPERIMENTAL MODEL AND SUBJECT DETAILS

Mouse lines

Cx3cr1-Cre mice were obtained from TAAM Orléans and bred to maintain them on the C57Bl/6J background. The mGcm2flox/flox line was created at the Institute Clinique de la Souris (ICS, Strasbourg) (Figure 1A). Conditional knock-out (cKO) mice with their littermate controls derived from Cx3cr1-Cre/+;mGcm2flox/+ males were crossed with mGcm2flox/flox females. The open field behavioural test was conducted at the ICS.

To generate tamoxifen-inducible conditional knock-out mGcm2 mice specifically in microglia, $CX_{3CR1}^{CreER/+}$ knock-in mice (Parkhurst et al., 2013; JAX stock #021160) were crossed with mGcm2flox/flox mice. $CX_{3CR1}^{CreER/+}$;mGcm2flox/+ mice were crossed with mGcm2flox/flox animals to generate $CX_{3CR1}^{CreER/+}$;mGcm2flox/flox mice (called icKO thereafter) and $CX_{3CR1}^{CreER/+}$;mGcm2flox/+ (control). WT and mGcm2flox/flox were also used as controls for demyelinating lesion experiments. All mice were maintained on a normal diet in a 12-hour light/dark cycle. 5 to 10 mice were used per group (per gender, age and genotype).

For the aging studies mice were sacrificed at postnatal day 14 (P14), 2,12 and 24 months and for the LPC injection mice were at 10 to 16 weeks old.

All animal experiments were conducted according to the European law for the welfare of animals. All animal procedures were reviewed and approved by the "Comités d'Ethiques en Expérimentation Animale" of IGBMC-ICS and of the Paris Brain Institute - ICM.

MS tissue samples

Snap frozen post-mortem brain and cerebellar samples from MS and control patients were obtained from the UK MS tissue bank (Imperial College, London, registered charity 207495). Informed consent had been obtained from each patient and all procedures used by the Tissue Bank in the procurement, storage and distribution of tissue have been approved the London Multicentre Research Ethics Committee (MREC/02/2/39). For this study, we used 4 MS and 1 control samples (Table S2).

METHOD DETAILS

Genotyping

DNA were extracted according to the Jacks Lab protocol. For primers, we used: CX3Cr1cre GTTCGCAAGAACCTGATGGACA and CTAGAGCCTGTTTTGCACGTTC, mGcm2flox CAATAGGGAAGTGATCCCTAGAGTC and GGGAAACTTGTCTGTTCTTTCACACAG

and mGcm2WT CAATAGGGAAGTGATCCCTAGAGTC and GGGAAACTTGTCTGTTCTTTCACACAG, forward and reverse, respectively. Primer sequences for Cx3cr1CreER genotyping were: CX3 F- CTTCTTGCGATTCTTGCAGG; CX3 R -CACTACCTCAT CATCCATGA; CX3CreER1- CACGGGGGAGGCAGAGGGTTT; CX3CreER2-GCGGAGCACGGGCCACATTTC.

Tamoxifen treatment

To induce Cre recombination, adult Cx3cr1CreER/+;mGcm2flox/flox and Cx3cr1CreER/+; mGcm2flox/+ mice (10 to 16week-old) were treated with tamoxifen (100 mg/kg; Sigma) by intraperitoneal injections, during 5 consecutive days prior LPC-induced demyelination.

LPC-induced demyelination of the mouse spinal cord

C57Bl6/J 12week-old females from Janvier were used for focal spinal cord demyelinated lesions. To evaluate microglial response and oligodendrocyte differentiation, we used tamoxifen treated Cx3cr1CreER/+;mGcm2flox/flox, Cx3cr1CreER/+;mGcm2flox/+, Gcm2flox/flox and WT mice. Twenty minutes before anaesthesia induction with 3% Isoflurane, animals were injected with Buprenorphine (0.1 mg/kg). After induction, isoflurane concentration was increased to 2% for the surgical phase. Animals were placed on the stereotaxic frame, and small incision was made at the level of thoracic vertebrae (T8 and T9). Using a Hamilton syringe connected with a glass capillary, 1% lyso-phosphatidylcholine (LPC, sigma) was injected into the dorsal funiculus of the spinal cord. The injection site was marked with an active charcoal, and internal and external sutures were made. After surgery, animals were injected subcutaneously with Buprenorphine during 2 consecutive days and then treated ad libitum with a solution of Buprenorphine in the drinking water.

P1 primary CNS cultures

Postnatal day 1 (P1) cultures were produced as previously described (Parkhurst et al., 2013). The cultures were kept in the incubator at 37°C and 5 % CO2 for 14 days. The medium was changed at day 1 and day 3. *In vitro* cultures were fixed with 4 % PFA (Electron Microscopy Sciences) in PBS 0.1M and then proceed to the immunolabeling.

Tissue dissections

Mice were anesthetised by a solution of Ketamine (100 mg/mL)/Xylazine (Rompun, 20 mg/mL): 130 mg/kg of ketamine + 13 mg/kg of xylazine, transcardially perfused with ice-cold PFA 4% in 0.1M PBS, and then the brains, the spinal cord, lungs and adipose tissue were dissected. The tissues were fixed overnight with 4% PFA in 0.1M PBS and then the brains were cut into left and right hemisphere, the rest of the tissues were cut in half. Half of the samples were embedded with paraffin and the other half with cryomatrix. 8 μm and 50 μm thick sections were used for paraffin labelling and for cryo-section, respectively.

For LPC demyelinated lesions, mice were euthanised several days post LPC-injection (dpi), after lethal anaesthesia with Xylazine (10 mg/kg) and pentobarbital sodium (150 mg/kg), and then transcardially perfused 4% PFA in 0.1M PBS. Spinal cords were dissected and post-fixed 2 h in 4% PFA. After post-fixation, spinal cords were cryoprotected in 20% sucrose solution O/N and then frozen in O.C.T. compound (Thermo Fisher) at −60°C in isopentane. Coronal spinal cords were sections (12 μm thickness) were performed at cryostat (Leica) and slides were kept on −80°C until use.

Immunolabelling in mouse samples

For immunolabeling, samples were permeabilized with PTX (0.1M PBS, 0.1% Triton-X100) for 30 min and incubated with blocking buffer for 1 h at room temperature (RT). The samples were incubated with primary antibodies overnight at 4°C, then incubated with the appropriate secondary antibodies. Finally, they were incubated with DAPI, (Sigma-Aldrich)) to label the nuclei and the samples were mounted with Aqua Poly/Mount (Polysciences). Primaries and their appropriate secondary antibodies are on Table S1.

For peroxidase immunolabelling of Iba1, sections were incubated with the primary antibody incubation overnight and then washed extensively in 0.1M PBS,0.1% Triton. Slides were incubated for 1 h in RT with biotinylated secondary antibody for 1 h, washed extensively and then incubated with the avidin–biotin–peroxidase (ABC) complex (Vector Laboratories). After washes, slides were incubated with the chromogen 3,3′ diaminobenzidine tetrahydrochloride (DAB; Sigma–Aldrich) until desired labelling intensity developed and counterstained with haematoxylin.

Oil red O staining

For Oil Red O (ORO) that labels macrophages containing myelin debris, spinal cord sections were dried at RT, rinsed in 60% isopropanol, then stained with freshly prepared and filtered 0.01% ORO solution. After 20 min, slides were rinsed in 60% isopropanol, counterstained with haematoxylin, rinsed in water and mount in aqueous mounting medium.

MS tissue samples

Snap frozen post-mortem brain and cerebellar samples from MS and control patients were cut into 12μm-thick sections on a cryostat, and lesions were classified as active (N = 2), chronic active (N = 1) and chronic inactive (N = 2), using Luxol fast blue/major

histocompatibility complex class II (MHCII) staining, as previously described (Nait-Oumesmar et al., 2007). For immunohistochemistry, sections were post-fixed 20 min in 2% PFA and immunofluorescence labelling was performed as mentioned above for mouse experiments.

Quantitative RT-PCR analysis

Animals were euthanised by CO2 inhalation, and samples of spinal cords around of the injection site was dissected. Total RNA, from 4 dpi LPC- and saline-injected spinal cords, were purified using RNeasy Mini Kit (Qiagen 74104). RNA concentrations were measured using Nanodrop. Reverse transcription was performed by using High-capacity cDNA reverse transcription kit with RNase inhibitor (Applied Biosystem 4374967). qPCR was performed with the TaqMan Fast Advanced Master Mix (Thermo Fisher 4444556) with specific probes for Hprt, mGcm2, iNOS, TLR2, ARG1, Il-4ra, and CD16 (Table S2). qPCR reactions with the same concentration of cDNA were run in duplicates using LightCycler 96 (Roche). Hprt was used as a housekeeping gene and used as endogenous control. ΔCt values were used to determine the relative gene expression change.

RNAscope multiplex assay

RNAscope *in situ* hybridisation (RNA ISH) was performed on fixed frozen sections of mouse and human post-mortem samples. Preparations, pre-treatment and RNA ISH steps were performed according to the manufacturer's protocols. All incubations were at 40°C and used a humidity control chamber (HybEZ oven, ACDbio). For mouse experiments, probe mixes used were as follows: mCX3CR1 (Cat No.314221-C2), mGcm2 (Cat No. 530481-C3), mGcm1 (Cat No. 429661-C1), Polr2a (Cat No.312471, used a positive control) and dapB (No. EF191515; used a negative control). For RNA ISH on human tissues, probes used were: hGCM2 (Cat.871081), hCD68 (Cat.560591) and Polr2a (Cat No.310451, used as positive control); on Drosophila, we used the gcm probe (Cat No.1120751-C1)

Tyramide dye fluorophores (Cy3, Cy5: TSA plus; and Aykoya) or Opal fluorophores (Opal 520, Opal 570, Opal 690, Aykoya) were used diluted appropriately in RNAscope Multiplex TSA dilution buffer. Slides were also counterstained with DAPI.

Imaging

Fluorescent and brightfield imaging were performed under a 20X objective using Axioscan (Zeiss) and Nanozoomer (Hammamatsu) for all quantitative analysis, and representative images in the figures were made using an Apotome (Zeiss).

Leica Spinning Disk microscope equipped with 20, 40 and 63X objectives was used to obtain confocal images with a step size of 0.2–1 μm. For the quantifications, five or more fields per sample were used with more than 50 cells in total.

Transcriptome analysis of gcmKD haemocytes from *Drosophila* embryos and larvae

Haemocytes were sorted by FACS from stage 16 embryos of the following genotypes: srp(hemo)Gal4/+;UAS-RFP/+ for the control and srp(hemo)Gal4/+;UAS-RFP/UAS-gcm-RNAi (BDRC #31519) for the gcmKD (Cattenoz et al., 2020). Haemocytes were also sorted from wandering third instar larvae of the following genotypes: srp(hemo)Gal4/HmlΔRFP (control) and srp(hemo)Gal4/hmlΔRFP;UAS-gcm-RNAi/+ (BDRC #31519) for the gcmKD. 20000 to 50000 cells were sorted for each replicate, three replicates were done for each condition. The RNA were extracted using Tri-reagent (SigmaAldrich) according to the manufacturer protocol. RNAseq libraries were prepared using the SMARTer (Takara) Low input RNA kit for Illumina sequencing. All samples were sequenced in 50-length Single-Read. At least 40x106 reads were produced for each replicate. Data analysis was performed using the GalaxEast platform (http://www.galaxeast.fr/, RRID:SCR_006281) as described in (Afgan et al., 2018; Cattenoz et al., 2020). The differential expression analysis was carried out using HTseq-Count (RRID:SCR_011867) and DESeq2 (RRID:SCR_015687) (Anders et al., 2015). The gene ontology analysis was done with ShinyGO 0.76 (Ge et al., 2020). The graphs were plotted using the packages pheatmap (RRID:SCR_016418) and ggplot2 (RRID:SCR_014601) in R (version 3.4.0) (R Core Team, 2017). The RNAseq data were deposited in the ArrayExpress database at EMBL-EBI (www.ebi.ac.uk/arrayexpress) under accession number E-MTAB-8702.

Expression profile of the microglial markers in adult *Drosophila* haemocytes and glia

The dataset GSE79488 for adult haemocytes and GSE142788 for adult glia were retrieved from GEO database, mapped using RNA-STAR and compared with DESeq2 as described above. The microglial genes conserved across evolution were determined by Geirsdottir (Geirsdottir et al., 2019). The Drosophila orthologs were determined using DIOPT 67. The heatmap was drawn using pheatmap (RRID:SCR_016418).

Tracing *gcm* expression

To assess the induction of gcm expression in Drosophila upon wasp infestation, a lineage tracing system was expressed under the control of gcm-specific promoters and a thermosensitive inhibitor. The detailed genotype is UAS-FLP/+;act5c-FRT,y+,FRT-Gal4,UASmCD8GFP/gcmGal4,tubulinGal80TS;UAS-FLP,Ubi-p63E(FRT.STOP)Stinger/6KbgcmGal4 (gcm>g-trace) for the experiment and UAS-FLP/+; act5c-FRT,y+,FRT-Gal4,UASmCD8GFP/+; UAS-FLP,Ubi-p63E(FRT.STOP)Stinger/+ for the control (Figure S4D). Embryos and larvae were raised at 18°C (tracing off) until the second instar larval stage, to avoid revealing the embryonic expression

of gcm. Second instar larvae were infested with the parasitoid wasp Leptopilina boulardi. 20 female wasps were used to infest 100 Drosophila larvae for 2 h at RT. Infested larvae were then transferred at 29°C (tracing on) and let develop until wandering third instar larval stage for further analyses.

Wasp infestation assays

Wasp eggs were collected upon bleeding 50 infested larvae in PBS 1X added with some N-Phenylthiourea crystals (Sigma) to prevent haemocyte melanisation. Wasp eggs were fixed in 4% PFA/PBS 1X for 30 min, washed with PTX (0.3% Triton X-100 in PBS 1X), incubated 1 h in PTXN (NGS 5% in PTX, Vector Laboratories), incubated overnight at 4°C in primary antibodies, washed with PTX, incubated 1 h in secondary antibodies, 1 h with DAPI and TRITC-phalloidin (Sigma), then mounted with Vectashield mounting medium (Vector Laboratories).

Haemocytes were labelled as previously published (Bazzi et al., 2018). Primaries and their appropriate secondary antibodies are on Table S1.

For the gain and loss of function assays, we used control, gain of function (GOF) or loss of function (LOF) flies upon crossing w;hmlΔGal4/CyoGFP;tubGal80TS animals with white-1118 (control), UASTgcmF18A (gain of function, GOF) or UASgcmRNAi (loss of function, LOF) animals, respectively (Flici et al., 2014). The infestation was conducted as described above and the tumour size was counted as previously described (Bazzi et al., 2018).

Adult CNS dissection

Flies were anesthetised with CO_2 and put on a silicone tray with 0.3% of PTX. The CNS was dissected out, fixed with 4% PFA 1xPBS overnight at 4°C, washed three times with PTX, incubated with blocking reagent for 2 h in RT, incubated overnight at 4°C with primary antibodies, washed three times for 10 min with PTX, incubated for 2 h with secondary antibodies, washed two times for 10 min with PTX, incubated for 20 min with DAPI and then mounted with Aqua Poly/Mount. The slides were analysed by confocal microscopy.

QUANTIFICATION AND STATISTICAL ANALYSIS

Image analysis

Image analysis was performed with the Fiji image analysis program and with Imaris. Fiji was mainly used to produce images with sum of Z-projections. In all images, the signal was set to the same threshold in order to compare the different genotypes. Imaris (version 9.5.1) was used to analyse the morphology of microglial cells during aging using a semi-automatic protocol. The p-values were estimated after comparing control to cKO cells by two-way ANOVA test followed by bilateral student test. To analyse the activation state of microglia in LPC lesions at 7 and 14 dpi, we used the Visiopharm software. We selected 2 parameters: the number of branching points (ramifications) and roundness. Data were analysed by two-way ANOVA, followed by Tukey post hoc test.

Statistical analysis

Variance analysis using bilateral student tests for unpaired samples was used to estimate the p-values for microglia ramifications, coverage area, iNOS, Arg1-positive microglia. In each case, at least five animals were counted. In all analyses, ''ns'' means not significant, ''*'' for p-value < 0.05; ''**'' for p-value < 0.01; ''***'' for p-value < 0.001.

For cell quantification in LPC lesions, 3–5 spinal cord sections per animal were analysed, with at least N = 3/group. Quantification of Olig2+ and CC1+ cells was performed using ZEN (Zeiss) and QuPath software. Statistical analyses were performed by using R and GraphPad (Prism) Software using Two-way ANOVA with Tukey post hoc comparison tests.

Cell Reports, Volume *41*

Supplemental information

An anti-inflammatory transcriptional cascade conserved from flies to humans

Alexia Pavlidaki, Radmila Panic, Sara Monticelli, Céline Riet, Yoshihiro Yuasa, Pierre B. Cattenoz, Brahim Nait-Oumesmar, and Angela Giangrande

Supplementary Figure Titles and Text:

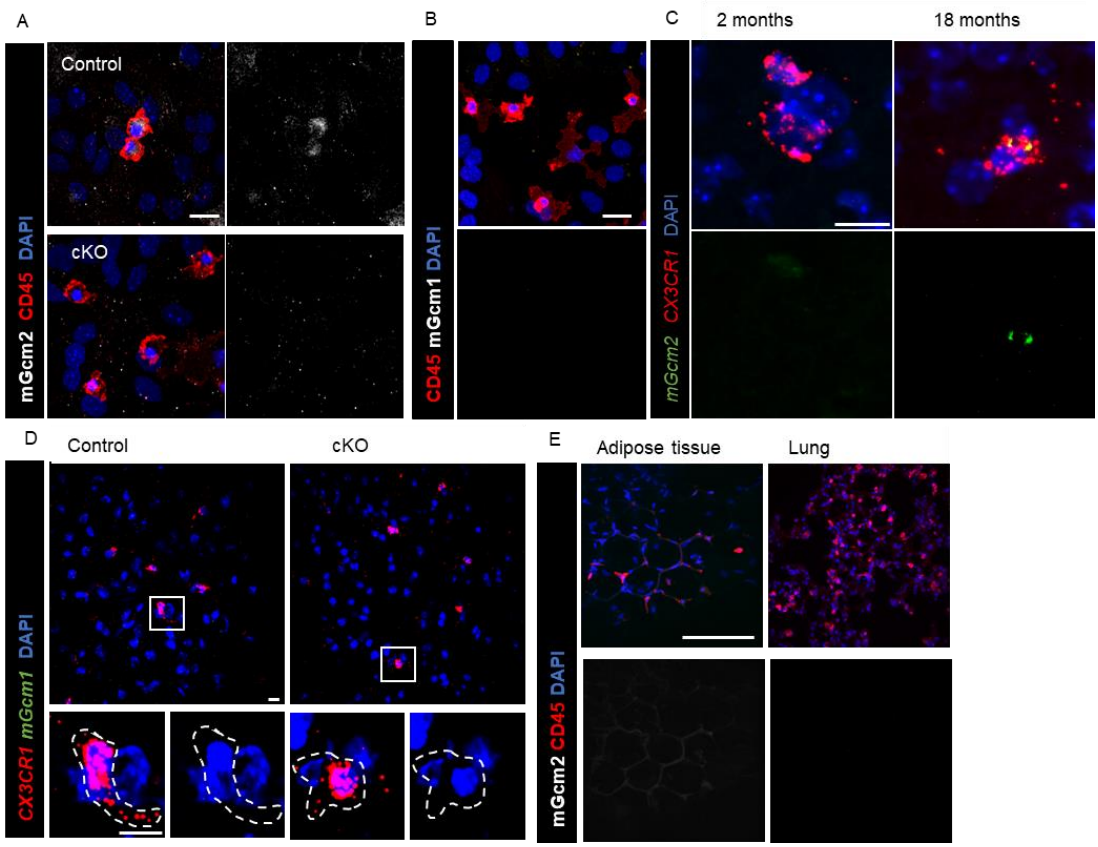

Figure S1. **mGcm1 and mGcm2 expression, Related to Figure 1**. (**A**) Immunolabelling of CNS primary cultures with CD45 (red), DAPI (blue) and mGcm2 (grey), N=3; scale bar: 10 µm. (**B**) Immunolabelling of CNS primary cultures for mGcm1 (grey), microglia (CD45, red) and DAPI (blue), N=3; scale bar: 10 µm. (**C**) RNA ISH of brain sections on P14, 2 and 18month-old brain sections from control and cKO animals: *Cx3cr1* (red), *mGcm2* (green) and DAPI (blue), N=3; scale bar: 10 µm. (**D**) RNAscope labelling on control and cKO brain sections at 18 months: *Cx3cr1* (red), *mGcm1* (green), DAPI (blue), N=3; scale bar: 10 µm. (**E**) Immunolabelling of resident macrophages from lung and adipose tissues at 24month-old animals: mGcm2 (grey), CD45 (red) and DAPI (blue). Scale bar: 100 µm.

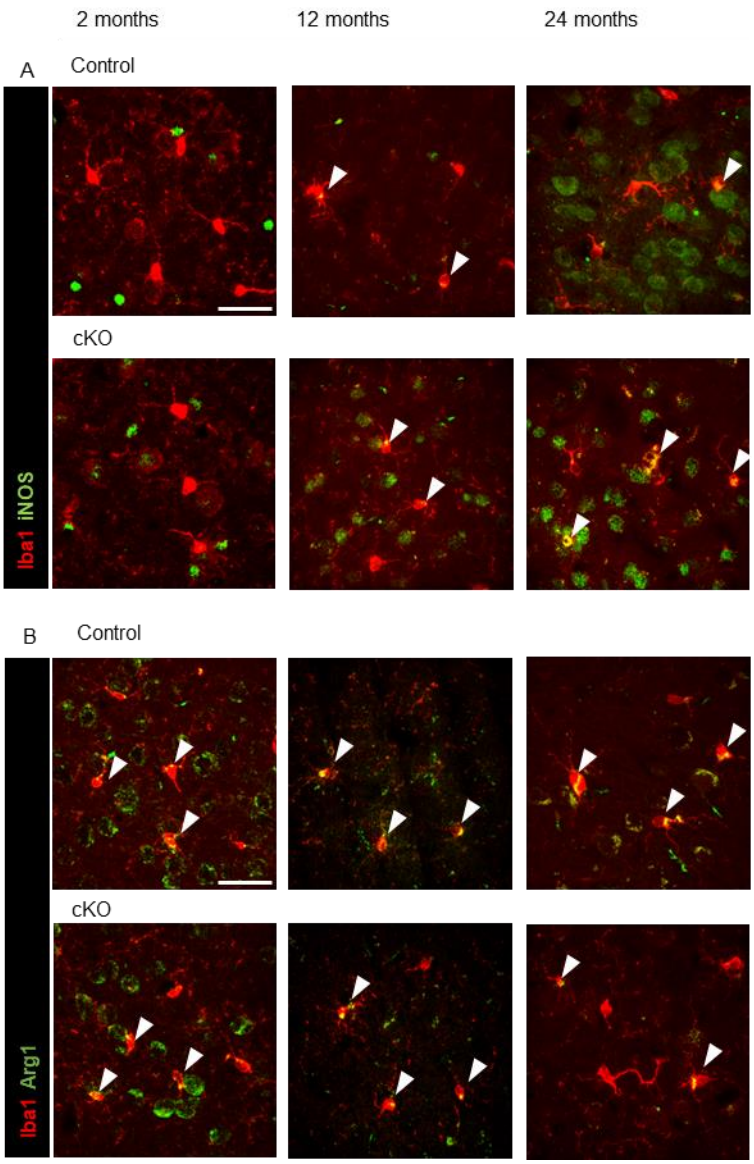

Figure S2. **Impact of mGcm2 deletion on microglia expression of inflammatory markers *in vivo*, Related to Figure 1.** (**A**) Immunolabelling of *in vivo* brain sections with the pro-inflammatory marker iNOS (green) and Iba1 (red), (**B**) Immunolabelling of *in vivo* brain sections with the anti-inflammatory marker Arg1 (green) and Iba1 (red), Double positive cells with Iba1 and iNOS or Arg1 expression are indicated by arrows. N=5-13; scale bar: 50 µm. *Cx3cr1-Cre+/-;mGcm2flox/+* (control) and *Cx3cr1-Cre+/-, mGcm2flox/flox* (cKO).

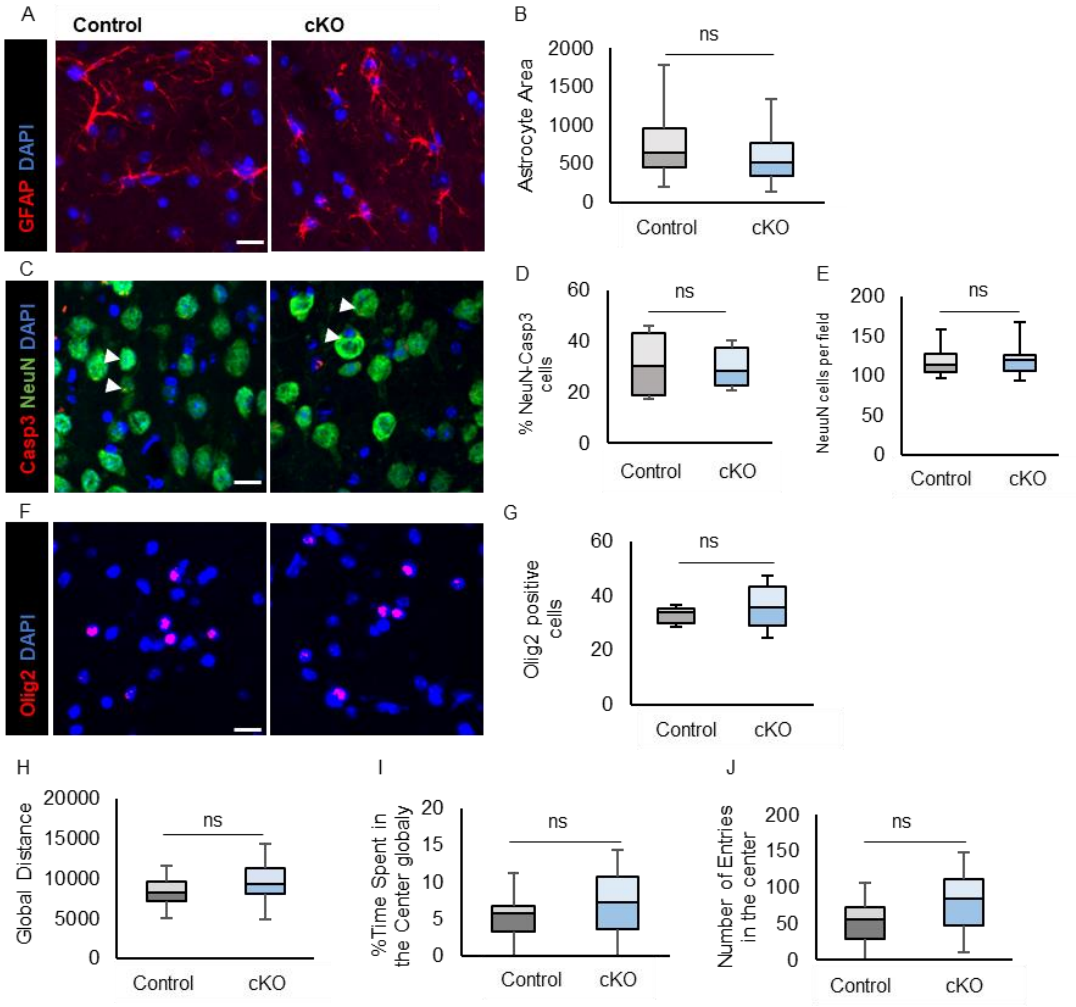

Figure S3. Characterisation of cell populations in the cortex of 24month-old animals, Related to Figure 1. (**A**) Immunolabelling of astrocytes from control and cKO animals for GFAP (red). (**B**) Quantification of the GFAP area. (**C**) Immunolabelling of neurons with the pan-neuronal marker NeuN (green) and the cell death marker Caspase3 (red). (**D**) Quantification of double positive NeuN-Caspase3 cells to calculate the neuronal cell death and (**E**) the total neuronal number. (**F**) Immunolabelling for oligodendrocytes with Olig2 and (G) quantification of oligodendrocytes in control and cKO animals. (**H,J**) Open field test for control and cKO animals at 18 months. The animals were evaluated for the total distance covered (**H**), the percentage of time spent in the centre (**I**) and how many times they entered in the centre (**J**). p-value: *<0.05, **<0.01, ***<0.001, and ns for not significant. N=5-13; scale bar: 50 μm. Statistical significance was determined by one-way ANOVA followed 2-tailed, unpaired t-test. *Cx3cr1-Cre*$^{+/-}$*;mGcm2*$^{flox/+}$ (control) and *Cx3cr1-Cre*$^{+/-}$*, mGcm2*$^{flox/flox}$ (cKO).

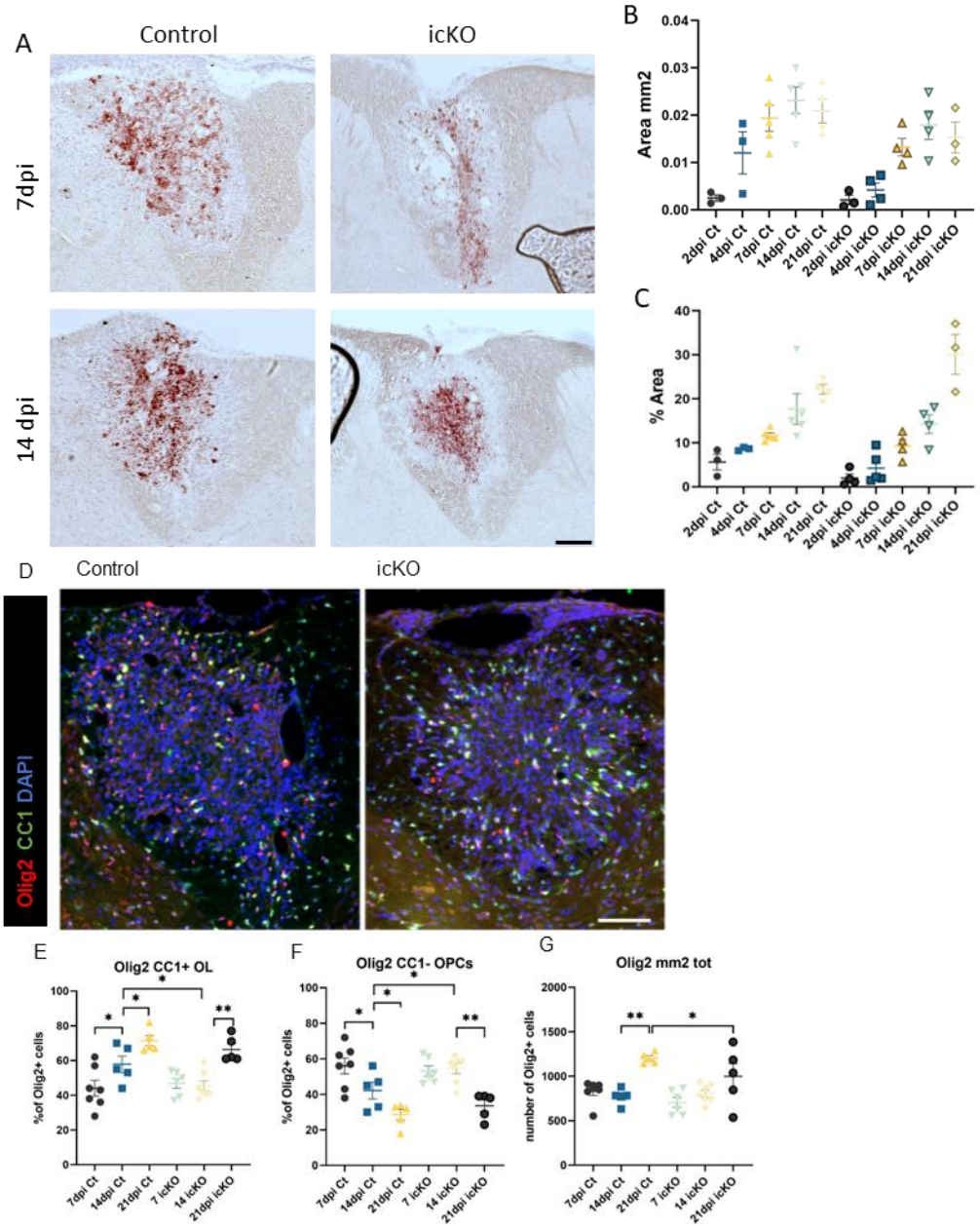

Figure S4. The impact of mGcm2 in microglia/macrophage phagocytosis and oligodendrocyte differentiation in LPC demyelinated lesions of *mGcm2* icKO mice, Related to Figure 3. (A) Oil-Red O staining of macrophages with myelin debris in control and *mGcm2* icKO LPC lesions, at 7 and 14 dpi. (**B**) Quantification of Oil-Red-O+ area in LPC lesions from 2 to 21 dpi, in control and *mGcm2* icKO animals. (**C**) Percentage of Oil-Red-O+ area in LPC lesions from 2 to 21 dpi in both experimental groups. Note that the clearance of myelin debris by macrophages in demyelinated lesions is not altered in *mGcm2* icKO with respect to control mice. (**D**) Immunolabelling with Olig2 (red) and CC1 (green) in LPC lesions of the spinal cord at 14 dpi, in control and *mGcm2* icKO mice. Nuclei are counterstained with DAPI. (**E,F**) Graphs indicating the percentage of Olig2/CC1-double positive differentiated oligodendrocytes and Olig2-positive/CC1-negative OPCs in demyelinated lesions from 7 to 21 dpi, in control and *mGcm2* icKO mice. (**G**) Quantification of the number of total Olig2-positive oligodendroglia in LPC lesions at 7, 14 and 21 dpi, in control and *mGcm2* icKO

animals. Two-way ANOVA followed by Tukey's multiple comparison tests were used for statistical analysis. *p< 0.05, **p< 0.01. Scale bar: (**A**), 100 μm (**D**), 100 μm.

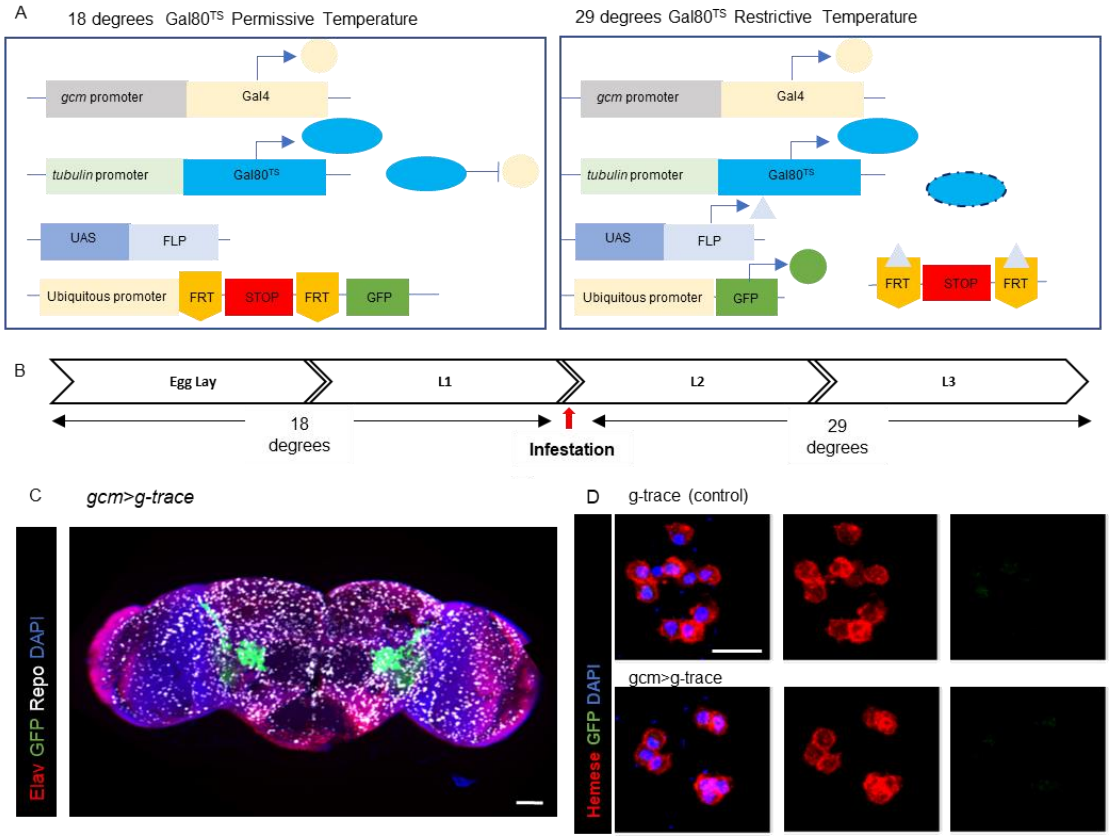

Figure S5. An inducible system tracing *gcm* expression, Related to Figures 5 and 6. (**A**) Inducible lineage tracing using the UAS-Gal4 system. The thermosensitive Gal80 protein ($Gal80^{TS}$) blocks Gal4 activity and hence Gal4-dependent gene transcription at 18°C. At 29°C, $Gal80^{TS}$ is rapidly degraded and Gal4-dependent transcription can occur, FLP indicates the Flippase recombinase, FRT the Flippase Recognition Target. (**B**) Timeline of the wasp infestation assay. Larvae were kept at 18°C and upon infestation they were transferred at 29°C until the end of the larval development. (**C**) Immunolabelling of adult *Drosophila* brain with *gcm* tracing (*gcm>g-trace*=GFP) in green, Repo (white), Elav (white) and DAPI (blue). (**D**) Immunolabelling of haemocytes from control (g-trace) and *gcm*>g-trace strains. The pan-haemocyte marker Hemese (red), g-trace (green), DAPI (blue). Animals were raised at 18°C and shifted at 29°C at second larval instar. Scale bar: 20 µm.

Table S1. MS and control cases used to study hGCM2 expression. Related to Figure 4

MS cases	**Age**	**Sex**	**PMD**	**Disease duration**	**Disease course**	**Lesions analyzed**			
						Active	Chronic active	Chronic inactive	Shadow plaques
MS94CLA6	42	F	11	6	PP	**1**			
MS100CLC2	46	M	7	8	SP			**1**	
MS121CLC5	49	F	24	14	PR	**1**		**1**	
MS106L6C8	39	F	18	21	PP		**1**		
Control									
C26CLA5	79	F	18	Cardiac failure					

Table S2. Oligonoucleotides table, Related to Figures 3, 4 and 5.

Reagent or Resource	Source	Identifier
Oligonoucleotides		
HPRT TaqMan® Gene Expression Assays (Mm03024075_m1)	**in this paper**	**N/A**
GCM2 TaqMan® Gene Expression Assays (Mm00492312_m1)	**in this paper**	**N/A**
NOS2 TaqMan® Gene Expression Assays (Mm00440502_m1)	**in this paper**	**N/A**
TLR2 TaqMan® Gene Expression Assays (Mm00442346_m1)	**in this paper**	**N/A**
ARG1 TaqMan® Gene Expression Assays (Mm00475988_m1)	**in this paper**	**N/A**
IL-4a TaqMan® Gene Expression Assays (Mm01275139_m1)	**in this paper**	**N/A**
Cd163 TaqMan® Gene Expression Assays (Mm00474091_m1)	**in this paper**	**N/A**
mCX3CR1	**ACD Bio**	**Cat No.314221-C2**
mGcm2	**ACD Bio**	**Cat No. 530481-C3**
mGcm1	**ACD Bio**	**Cat No. 429661-C1**
mPolr2a	**ACD Bio**	**Cat No.312471-C2**
dapB	**ACD Bio**	**Cat No 310043-C2**
hGCM2	**ACD Bio**	**Cat 871081-C1**
hCD68	**ACD Bio**	**Cat.560591-C2**
hPolr2a	**ACD Bio**	**Cat No.310451-C1**
Drosophila *gcm*	**ACD Bio**	**Cat No.1120751-C1**